The signaling lipid sphingosine 1-phosphate regulates mechanical pain

Authors and Affiliations: Rose Z. Hill[1], Benjamin U. Hoffman[2, 3], Takeshi Morita[1#], Stephanie M. Campos[4‡], Ellen A. Lumpkin[2, 4], Rachel B. Brem[5, 6], Diana M. Bautista[1, 4, 7, 8*]

1. Department of Molecular and Cell Biology, University of California, Berkeley, CA 94720, USA.
2. Department of Physiology & Cellular Biophysics, Columbia University College of Physicians & Surgeons, New York, NY 10032
3. Medical Scientist Training Program, Columbia University, New York, NY 10032
4. Neurobiology Course, Marine Biological Laboratory, Woods Hole, MA
5. Department of Plant and Microbial Biology, University of California, Berkeley, CA 94720, USA.
6. Buck Institute for Research on Aging, Novato, CA 94945, USA.
7. Helen Wills Neuroscience Institute, University of California, Berkeley, CA 94720, USA.
8. Corresponding author

[#] Current Address: Rockefeller University, New York, NY 10065, USA.

[‡] Current Address: Indiana University, Bloomington, IN 47405, USA.

* Correspondence: dbautista@berkeley.edu

Abstract

Somatosensory neurons mediate responses to diverse mechanical stimuli, from innocuous touch to noxious pain. While recent studies have identified distinct populations of A mechanonociceptors (AMs) that are required for mechanical pain, the molecular underpinnings of mechanonociception remain unknown. Here, we show that the bioactive lipid sphingosine 1-phosphate (S1P) and S1P Receptor 3 (S1PR3) are critical regulators of acute mechanonociception. Genetic or pharmacological ablation of S1PR3, or blockade of S1P production, significantly impaired the behavioral response to noxious mechanical stimuli, with no effect on responses to innocuous touch or thermal stimuli. These effects are mediated by fast-conducting A mechanonociceptors, which displayed a significant decrease in mechanosensitivity in S1PR3 mutant mice. We show that S1PR3 signaling tunes mechanonociceptor excitability via modulation of KCNQ2/3 channels. Our findings define a new role for S1PR3 in regulating neuronal excitability and establish the importance of S1P/S1PR3 signaling in the setting of mechanical pain thresholds.

Introduction

Pain is a complex sensation. It serves to protect organisms from harmful stimuli, but can also become chronic and debilitating following tissue injury and disease. Distinct cells and molecules detect noxious thermal and mechanical stimuli. Thermal pain is detected by thermosensitive TRP channels in subsets of nociceptors[1,2], and gentle touch is detected by Piezo2 channels in low-threshold mechanoreceptors (LTMRs)[3,4]. Aδ high-threshold mechanoreceptors (HTMRs) have been shown to play a key role in responses to painful mechanical stimuli[5,6].

Recent studies have shown that there are at least two populations of HTMRs that mediate responses to noxious mechanical stimuli. The *Npy2r*$^+$ subpopulation of HTMRs mediates fast paw withdrawal responses to pinprick stimulation and terminates as free nerve endings in the epidermis[5]. The *Calca*$^+$ subpopulation of circumferential-HTMRs responds to noxious force and hair pulling, and terminates as circumferential endings wrapped around guard hair follicles[6]. Additionally, somatostatin-expressing interneurons of laminae I-III in the dorsal horn of the spinal cord receive input from nociceptors and are required for

behavioral responses to painful mechanical stimuli[7]. Despite these advances in defining the cells and circuits of mechanical pain, little is known about the molecular signaling pathways in mechanonociceptors.

Here, we show that sphingosine 1-phosphate (S1P) is required for mechanical pain sensation. S1P is a bioactive lipid that signals via 5 G-protein coupled S1P Receptors (S1PRs 1-5). S1P signaling, mainly via S1PR1, plays a well-known role in immune cell migration and maturation[8–10]. Additionally, recent studies have shown that S1PRs are expressed throughout the nervous system[11–13] and S1P signaling is associated with a variety of neuroinflammatory disorders, including multiple sclerosis[14] and Alzheimer's disease[15]. S1P has been implicated in spontaneous pain[13] and thermal pain hypersensitivity[12,16,17], but due to conflicting accounts of S1P receptor expression in the CNS[11,18] and PNS[12,13,19] as well as inconsistent reports on the effects of S1P on neuronal excitability[13,20,21] and pain behaviors[12,13,16,17], the role of S1P in somatosensation remains controversial.

We found that mice lacking the S1P receptor S1PR3 display striking and selective deficits in behavioral responses to noxious mechanical stimuli. Likewise, peripheral blockade of S1PR3 signaling or S1P production impairs mechanical sensitivity. We show that S1P constitutively enhances the excitability of A mechanonociceptors (AMs) via closure of KCNQ2/3 potassium channels to tune mechanical pain sensitivity. The effects of S1P are completely dependent on S1PR3. While previous studies have shown that elevated S1P triggers acute pain and injury-evoked thermal sensitization[12,13], we now demonstrate that baseline levels of S1P are necessary and sufficient for setting normal mechanical pain thresholds. By contrast, elevated S1P selectively triggers thermal sensitization via activation of TRPV1$^+$ heat nociceptors, with no effect on mechanical hypersensitivity. Our findings uncover an essential role for constitutive S1P signaling in mechanical pain.

Results

To identify candidate genes underlying mechanosensation, we previously performed transcriptome analysis of the sensory ganglia innervating the ultra-sensitive tactile organ (the star) of the star-nosed mole[22]. Immunostaining revealed the tactile organ is preferentially innervated by myelinated Aδ fibers[22],

which are primarily mechanosensitive. While our original analysis focused on ion channels enriched in the neurons of the star organ, our dataset also revealed enrichment of several components of the S1P pathway, including *S1pr3*. Likewise, single-cell RNA seq of mouse dorsal root ganglion (DRG) neurons revealed *S1pr3* expression in a subset of myelinated mechanoreceptors[19] in addition to a subpopulation of peptidergic C nociceptors.

S1P promotes excitability in small-diameter, capsaicin-sensitive nociceptors[12,13,20,21]. In addition, S1PR3 has been shown to mediate spontaneous pain triggered by elevated S1P and thermal sensitization following sterile tissue injury[13]. However, no studies have examined the role of S1PR3 in mechanosensation or in regulating somatosensory behaviors under normal conditions. Given the enrichment of *S1pr3* in mechanosensory neurons of the star-nosed mole and mouse, we hypothesized that S1P signaling via S1PR3 may also play a role in mechanosensation. Thus, we set out to define the role of S1P signaling and S1PR3 in somatosensory mechanoreceptors.

S1PR3 mediates acute mechanical pain

We first examined a variety of somatosensory behaviors in mice lacking S1PR3[23] (*S1pr3*$^{tm1Rlp/Mmnc}$*;* referred to herein as S1PR3 KO). We initially investigated baseline responses to mechanical stimuli. S1PR3 KO mice displayed a dramatic loss of mechanical sensitivity (**Figure 1A; see Figure 1-source data 1**), as von Frey paw withdrawal thresholds were significantly elevated in S1PR3 KO mice relative to WT and S1PR3 HET littermates (mean thresholds: 1.737 g vs. 0.736 and 0.610 g, respectively). Moreover, S1PR3 KO mice demonstrated decreased responses to a range of noxious tactile stimuli (2-6 g; **Figure 1B**) and to noxious pinprick stimulation (**Figure 1C**), but normal responsiveness to innocuous tactile stimuli (0.6-1.4g; **Figure 1B**). S1PR3 KO mice exhibited normal tape removal attempts[3] (**Figure 1D**), righting reflexes (**Figure 1-figure supplement 1A**), radiant heat withdrawal latencies (**Figure 1E**), and itch-evoked scratching (**Figure 1-figure supplement 1B**). These results demonstrate a selective role for S1PR3 in acute mechanical pain.

As a complement to our analysis of somatosensation in S1PR3 KO animals, we employed a

pharmacological approach, using the S1PR3-selective antagonist TY 52156 (TY)[24]. Similar to the phenotype of knockout animals, intradermal injection of 500 μM TY into the mouse hindpaw (the site of testing) triggered a rapid and significant elevation in von Frey paw withdrawal thresholds (**Figure 1F**) and decreased responsiveness to noxious (2-6 g), but not innocuous (0.6-1.4g), tactile stimuli (**Figure 1G**), without affecting noxious heat sensitivity (**Figure 1-figure supplement 1C**). By contrast, blockade of S1PR1 with the selective antagonist W146[16] had no effect on baseline mechanical or thermal thresholds (**Figure 1F; Figure 1-figure supplement 1C**). Overall, these data show that S1PR3 signaling sets mechanical pain sensitivity.

Endogenous S1P mediates acute mechanical pain

We next asked whether peripheral S1P was required for the S1PR3-dependent effects on mechanosensation. We decreased S1P levels via injection of the sphingosine kinase inhibitor SKI II to block local production of S1P[25] or elevated S1P levels via intradermal injection of S1P and measured behaviors 30 minutes after injection. Decreasing local S1P levels with SKI II significantly reduced mechanical sensitivity (**Figure 2A; see Figure 2-source data 1**), comparable to the hyposensitivity phenotype observed in S1PR3 KO mice (**Figure 1A**). Again, similar to what was observed in S1PR3 KO animals (**Figure 1E**), peripheral blockade of S1P production had no effect on baseline thermal sensitivity (**Figure 1-figure supplement 1C**). Surprisingly, injecting exogenous S1P (10 μM; maximum solubility in saline vehicle) had no effect on mechanical sensitivity (**Figure 2A-B**). However, as previously reported[12,13], S1P injection triggered S1PR3-dependent thermal hypersensitivity and spontaneous pain (**Figure 2C-D**), demonstrating that the lack of effect on mechanical hypersensitivity is not due to problems with S1P delivery or degradation.

These data support a model whereby S1P constitutively activates S1PR3 to set normal mechanical pain thresholds. To further test this model, we asked if the mechanical hyposensitivity elicited after endogenous S1P depletion (via SKI II) could be rescued by local injection of exogenous S1P. Indeed, we found that injection of exogenous S1P reversed SKI II-induced mechanical hyposensitivity in a dose-dependent manner, and observed a maximal effect with 200 nM S1P (**Figure 2E**). Although quantification of native

S1P levels in skin is inaccurate owing to avid lyase activity[26], our data establish that baseline S1P levels are sufficient to maximally exert their effect on S1PR3-dependent mechanical pain, such that increased S1P does not evoke mechanical hypersensitivity, but diminished S1P leads to mechanical hyposensitivity. These data show that constitutive activation of S1PR3 by S1P is required for normal mechanosensitivity.

S1PR3 is expressed in A mechanonociceptors and thermal nociceptors

Our behavioral data showing distinct roles for S1PR3 in mechanonociception and thermal hypersensitivity suggest that S1PR3 is expressed in distinct subsets of somatosensory neurons. While a previous study suggested that all somatosensory neurons express S1PR3[13], single cell RNA seq data suggests *S1pr3* is not expressed by all DRG neurons[19], and no studies have performed quantitative analysis of S1PR3 staining or co-staining to define subpopulations of S1PR3$^+$ neurons. We thus set out to characterize the somatosensory neuron subtypes expressing *S1pr3* using *in situ* hybridization (ISH) of wild-type somatosensory ganglia and immunohistochemistry (IHC) in an *S1pr3*$^{mCherry/+}$ reporter mouse[27].

We first used *in situ* hybridization (ISH) with a specific *S1pr3* probe to examine expression patterns of *S1pr3* (**Figure 3A-B**; see **Supplementary File 1**). In our experiments, 43% of cells from wild-type DRG expressed *S1pr3*. Co-ISH revealed that one population of *S1pr3*$^+$ neurons represents Aδ mechanonociceptors (AMs). These cells expressed *Scn1a* (39.9% of all *S1pr3*$^+$), a gene that encodes the Nav1.1 sodium channel, which mediates mechanical pain in Aδ fibers[28]. *S1pr3*$^+$ cells also co-expressed *Npy2r* (20.4% of all *S1pr3*$^+$), a marker of a subset of mechanonociceptive A fibers[5]. *S1pr3* was expressed in 70.6% of *Scn1a*$^+$ cells and 72% of *Npy2r*$^+$ cells, comprising a majority of both of these populations. Interestingly, a subset of cells co-expressed *S1pr3* and the mechanically sensitive channel *Piezo2*, which is expressed by Aβ, Aδ, and C fibers[3]. The remaining *S1pr3*$^+$ cells were *Trpv1*$^+$ and/or *Trpa1*$^+$ C nociceptors (67.1% of all *S1pr3*$^+$), which are reported to overlap minimally with the *Scn1a*$^+$ and *Npy2r*$^+$ populations[5,28].

We next used an *S1pr3*$^{mCherry/+}$ reporter mouse, which produces a functional S1PR3-mCherry fusion protein[27], as an independent strategy to explore S1PR3 expression and localization. This strategy was used because we found that anti-S1PR3 antibodies showed broad immunoreactivity in DRG from mice lacking S1PR3, and so we instead used anti-DsRed antibodies to probe expression of the S1PR3 fusion

protein (**Figure 3-figure supplement 1E**). We found that 42.4% S1PR3$^+$ cells co-stained with anti-Peripherin, demonstrating that S1PR3 is expressed in a subset of small-diameter neurons. We also observed that 69.5% of S1PR3$^+$ cells co-stained with anti-NF200, which marks medium and large-diameter myelinated neurons. Furthermore, we observed that S1PR3$^+$ cells were primarily of small to medium diameter (11.3-35.1 µm), whereas all cells in the DRG ranged from 11.3-53.9 µm. Overall, these data support the expression of S1PR3 in subsets of small-diameter thermal nociceptors and medium-diameter mechanonociceptors (**Figure 3F**). Additionally, no significant differences were observed between WT and S1PR3 KO DRG in number of *Trpa1, Trpv1,* Peripherin-, NF200-, or IB4-positive cells (**Figure 3-figure supplement 1B-C, F, G**). The mean diameters of *Trpv1*$^+$ neurons (**Figure 3-figure supplement 1D**, left), NF200$^+$ neurons (**Figure 3-figure supplement 1G**), or all neurons (**Figure 3-figure supplement 1D**, right) in WT versus KO DRG were not significantly different, suggesting no loss of major sensory neuronal subtypes in the S1PR3 KO.

We then visualized S1PR3 expression in nerve fibers that innervate the skin using anti-DsRed antibodies in whole-mount immunohistochemistry (IHC; **Figure 3D**). The reporter animals showed no specific antibody staining in epidermal or dermal cells (**Figure 3-figure supplement 1I**), and single-cell RNA seq of a diverse array of mouse epidermal and dermal cells corroborates this lack of expression[29]. We observed overlap of S1PR3-expressing free nerve endings with NF200-positive myelinated free nerves and NF200-negative putative C-fiber endings (**Figure 3F**), but did not observe expression of S1PR3 in NF200-positive circumferential or lanceolate hair follicle receptors, or in putative Merkel afferents (**Figure 3D-E**). β-tubulin III, PGP9.5 (pan-neuronal markers), and NF200 staining in S1PR3 KO skin displayed patterns of epidermal and dermal innervation similar to WT skin, suggesting the phenotypes observed in the S1PR3 KO mice are not due to developmental loss of sensory neuronal innervation ($p_{PGP9.5}$ = 0.443 (n = 93, 38 fibers); p_{NefH} = 0.405 (n = 61, 28 fibers); p_{BTIII} = 0.353 (n = 104, 89 fibers); two-tailed t-tests based on average number of fibers per field of view). These results support expression of S1PR3 in subsets of myelinated A mechanonociceptors and unmyelinated C nociceptors that terminate as free nerve endings.

S1P activates thermal nociceptors but not putative AMs

Live imaging of cultured DRG neurons from adult reporter animals showed expression of S1PR3-mCherry fusion protein in 48.3% of neurons, mirroring our ISH and IHC results (**Figure 4A**). To examine the effects of S1P on A mechanonociceptors and C nociceptors, we performed ratiometric calcium imaging and electrophysiology on DRG cultures from reporter mice. Interestingly, only 56.1 ± 22.4 % of mCherry-expressing neurons were activated by 1 µM S1P (Representative trace in **Figure 4B**; representative images in **Figure 4C**), which our dose-response showed to be the saturating concentration for calcium influx (**Figure 4D**; EC_{50} = 155 nM). All S1P-responsive neurons were also capsaicin-sensitive (n > 2000 neurons). And while sensory neurons from S1PR3 KO animals did not respond to S1P, as expected[13], they exhibited capsaicin responses that were not significantly different from WT neurons (**Figure 3-figure supplement 1H**). The mean diameter of S1P-responsive mCherry$^+$ neurons was 22.4 ± 1.0 µm, whereas the mean diameter of non-responsive mCherry$^+$ neurons was 28.7 ± 3.2 µm (p = 0.0002, two-tailed t-test). We also performed whole cell current clamp experiments and, consistent with other studies[12,20,21], found that S1P evoked action potential firing in capsaicin-sensitive small diameter cells (**Figure 4E**). This shows that only the small-diameter, S1PR3$^+$ putative nociceptors are excited by S1P. We next asked whether the S1PR3$^+$ medium-large diameter neurons represent the mechanonociceptors observed by ISH (**Figure 3A**). To this end, we asked whether the spider toxin Hm1a, a selective activator of AM nociceptors[28], triggers calcium influx in S1PR3-expressing trigeminal neurons. Indeed, we found that 44.2 ± 15.1% of Hm1a-responsive neurons expressed mCherry (**Figure 4F**), consistent with our staining showing expression of *S1pr3* in AM nociceptors and the role of Hm1a-responsive neurons in mediating mechanical pain *in vivo*[28].

S1PR3 modulates KCNQ2/3 channels to regulate AM excitability

We next interrogated the molecular mechanism by which S1P signaling in AM nociceptors may regulate mechanical pain. We performed whole-cell current clamp on the medium-diameter *S1pr3*$^{mCherry/+}$ dissociated DRG neurons (membrane capacitance = 61.05 ± 1.92 pF), which did not display S1P-evoked calcium influx (**Figure 4B-C**). In these cells, 1 µM S1P application did not change membrane potential (**Figure 5-figure supplement 1A;** see **Figure 5-source data 1**) or elicit firing in the absence of current injection (**Figure 5-figure supplement 1A**; **Figure 5A**). However, S1P dramatically lowered the threshold to fire action

potentials (rheobase) in an S1PR3-dependent manner (**Figure 5A**, **Figure 5-figure supplement 1B**).

We then set out to determine the mechanism by which S1PR3 activity increases neuronal excitability using whole-cell voltage clamp recording. Previous studies showed that S1P excites capsaicin-sensitive nociceptors by increasing voltage-gated sodium currents and reducing steady-state potassium currents[20,21]. We found that S1P had no such effects on S1PR3^{+} medium-diameter cells (**Figure 5-figure supplement 1C-E**). By contrast, S1P triggered a robust increase in input resistance (**Figure 5B**), consistent with the closure of potassium channels. I-V analysis revealed that the current inhibited by S1P application was carried by potassium (**Figure 5C**). Additionally, S1P significantly reduced slow, voltage-dependent tail current amplitudes (**Figure 5-figure supplement 1F**; **Figure 5D** (top)) in an S1PR3-dependent manner (**Figure 5-figure supplement 1F**, center).

As tail currents in Aδ neurons are primarily mediated by KCNQ2/3 potassium channels[30,31], we postulated that S1P may alter tail currents through modulation of these channels. Furthermore, the above properties of the S1P-sensitive current were consistent with the reported electrophysiological properties of KCNQ2/3 channels in DRG neurons[30,32,33]. To address whether KCNQ2/3 channels mediated S1P-dependent neuronal excitability, we applied the KCNQ2/3-selective inhibitor XE 991 and found that it completely occluded the effects of S1P on tail current (**Figure 5D**). Similar results were observed with the related antagonist, linopirdine (**Figure 5D**). These findings are consistent with S1P/S1PR3-dependent inhibition of KCNQ2/3 in somatosensory neurons.

We also found that the effect of S1P on KCNQ2/3 currents was mediated by low levels of S1P, exhibiting an IC_{50} of 48 nM with saturation at 100 nM (**Figure 5-figure supplement 1G**). While S1P cannot be accurately measured in non-plasma tissues, this is similar to estimated levels of S1P in peripheral tissues[10,34], and to levels which rescued mechanosensitivity after local S1P depletion (**Figure 2E**). Thus, our *in vitro* IC_{50} supports our behavioral observations that baseline S1P levels are sufficient to maximally exert their effect on mechanical pain. In summary, our electrophysiological and behavioral observations support a model in which baseline S1P/S1PR3 signaling governs mechanical pain thresholds through

modulation of KCNQ2/3 channel activity in AM neurons (**Figure 8**).

S1PR3 is required for nociceptive responses of high-threshold AM nociceptors

Given the effects of S1P on putative AM neurons *in vitro* and the selective attenuation of baseline mechanical pain in S1PR3 KO animals, we hypothesized that S1PR3 would play a role in AM afferent function. To test this, we utilized *ex vivo* skin-nerve recordings to analyze the effects of genetic ablation of S1PR3 on AM afferents, which mediate fast mechanical pain sensation. S1PR3 HET animals were used as littermate controls because no significant differences were observed between S1PR3 WT and S1PR3 HET mice in any behavioral assay (**Figure 1**), and because force-response relationships are comparable between S1PR3 HET AM fibers and wild type AM recordings[28,35–38] (**Figure 6-figure supplement 1A;** see **Figure 6-source data 1**). Compared to S1PR3 HET, S1PR3 KO AM nociceptors displayed reduced sensitivity in their force-response relation (slope for HET versus KO: 50 Hz/N versus 35 Hz/N), as well as attenuated firing over the noxious, but not innocuous, range of mechanical stimulation (**Figure 6A**). Strikingly, the median von Frey threshold to elicit firing in AM nociceptors was significantly higher in S1PR3 KO animals (3.92 mN) compared to littermate controls (1.56 mN; **Figure 6B**). Furthermore, S1PR3 KO AM nociceptors displayed a right-shifted cumulative response curve to force-controlled stimuli (50% effective force for HET versus KO: 33.7 versus 60.0 mN; **Figure 6C**), consistent with the mechanonociceptive hyposensitivity observed *in vivo*. By contrast, neither AM conduction velocities nor the conduction velocity distributions of Aβ, Aδ, and C fibers differed between genotypes (**Figure 6D** and **Figure 6-figure supplement 1B**).

A recent study reported that A-nociceptors are composed of two genetically distinct neuronal populations that differ in conduction velocity and in adaptation properties[5] ("Adapting AM" versus "Non-adapting AM"). We next asked whether loss of S1PR3 signaling altered these AM subtypes. Adapting AM fibers responded more vigorously to dynamic (ramp) stimuli than to static (hold) stimuli, and displayed a mean dynamic firing frequency at least twofold greater than their static firing frequency[5] (**Figure 6E, upper traces**). By contrast, Non-adapting AM fibers often showed bursting during static stimulation, which resulted in similar firing rates during dynamic and static stimulation (**Figure 6E, lower traces**). S1PR3 KO

animals displayed a significantly lower proportion of Adapting AM nociceptors compared with littermate controls (**Figure 6F**). Additionally, we observed an increase in S1PR3 KO AM fibers that were unresponsive to controlled force stimulation (**Figure 6F**). These "non-responders" only fired action potentials to high-pressure stimuli with a blunt glass probe or to suprathreshold stimulation with von Frey filaments (see Methods). The Non-adapting AMs, and the few remaining mechanosensitive Adapting AMs in the S1PR3 KO displayed similar firing frequencies over both the dynamic and static phases of force application to control fibers (**Figure 6-figure supplement 1C**). This suggests that decreased mechanosensitivity of the Adapting AM population accounts for the significant reduction in force-firing relations observed at the population level in S1PR3 KO AMs (**Figure 6A**). We conclude that S1PR3 is an essential regulator of both mechanical threshold and sensitivity in a distinct population of AM nociceptors.

S1PR3 is required for inflammatory pain hypersensitivity

Having examined the mechanisms of S1P/S1PR3 signaling in acute mechanonociception, we next sought to evaluate S1P/S1PR3 signaling in pain hypersensitivity. For this purpose, we used an experimental model of inflammatory pain triggered by Complete Freund's Adjuvant (CFA) injection into the hindpaw, which elicits infiltration of immune cells and thermal and mechanical hypersensitivity[39]. While one previous study proposed that S1PR3 promotes injury-evoked heat and mechanical hypersensitivity, they did not measure or compare post-injury mechanical thresholds to pre-injury baselines for the knockout or control animals[13]. Here, we compared development of CFA-evoked hypersensitivity between S1PR3 HET and KO littermates, since no significant behavioral differences were observed between WT and HET animals in CFA experiments ($p_{\text{von Frey}} = 0.12$; $p_{\text{radiant heat}} = 0.12$; two-tailed *t*-tests). Strikingly, S1PR3 KO mice failed to develop thermal hypersensitivity (**Figure 7A;** see **Figure 7-source data 1**) relative to heterozygous littermates at both 24 and 48 hours post-CFA injection. In stark contrast, S1PR3 KO animals developed robust mechanical hypersensitivity when thresholds were normalized to account for the dramatic baseline differences between knockouts and control animals (**Figure 7B**). Our data demonstrate that S1PR3 mediates baseline mechanical sensitivity and is not required for the development of CFA-evoked mechanical hypersensitivity.

Influx of myeloid lineage ($Cd11b^+/Ly6G^-$) cells is required for the development of mechanical hypersensitivity in the CFA model[39]. In the immune system, S1P signaling via S1PR1 plays a key role in immune cell migration[9]. Consistent with the development of mechanical hypersensitivity, flow cytometry experiments showed robust infiltration of immune cells into hindpaw skin from both S1PR3 KO and littermate controls (**Figure 7-figure supplement 1A-B**). These data suggest that the phenotypes observed in S1PR3 KO mice cannot be attributed to compromised immune cell infiltration.

Next, we tested whether active S1P/S1PR3 signaling was required to maintain CFA-evoked thermal hypersensitivity using pharmacology. Acute blockade of S1P production with SKI II or S1PR3 with TY also reversed CFA heat hypersensitivity (**Figure 7C**), demonstrating that peripheral S1P actively signals via S1PR3 to promote CFA-evoked heat hypersensitivity. Furthermore, acute S1P/S1PR3 blockade with SKI II or TY elevated mechanical thresholds to pre-CFA, baseline levels (**Figure 7D**) showing that S1PR3 tunes mechanical pain under normal and inflammatory conditions. These results are consistent with the distinct roles for AM and C nociceptors in mechanical pain. Under normal conditions, AM nociceptors set mechanical pain thresholds[28,40]. By contrast, under inflammatory conditions, the combined activity of both non-sensitized AM fibers and sensitized C fibers determines overall post-inflammatory mechanical thresholds[41,40]. Consistent with this model, acute blockade of S1P production or S1PR3 activity under normal conditions induces mechanical hyposensitivity and under inflammatory conditions returns mechanical sensitivity to normal levels.

Discussion

We now show that S1P signaling via S1PR3 is a key pathway that tunes mechanical pain sensitivity. Overall, our data reveal two new key findings. First, S1P/S1PR3 sets baseline mechanical pain thresholds. Depletion of baseline, endogenous S1P induces mechanical hyposensitivity and nanomolar levels of exogenous S1P are sufficient to restore normal mechanical pain sensitivity after depletion. Second, elevated micromolar S1P levels, such as those produced during inflammation or disease, promote thermal, but not mechanical hypersensitivity. The effects of S1P on acute mechanical pain and thermal

hypersensitivity are completely lost in S1PR3 knockout animals, which are otherwise normal with respect to other somatosensory behaviors.

What is the local source of S1P in the skin that constitutively modulates mechanical pain? Even in the mature field of S1P signaling in the vascular and immune systems, the cellular source of S1P, while an intriguing question, remains unclear. All cells in the body, including somatosensory neurons, immune cells, and skin cells, express sphingosine kinases 1 and 2 which are essential for S1P production[42]. Deletion of both kinases is lethal and attempts to conditionally knockout these kinases fail to completely eliminate S1P in tissues[43]. While RNA seq data suggests that somatosensory neurons contain all of the enzymatic machinery required to produce and export local S1P[19,44], future work will be needed to identify the key cell types that are important for maintaining baseline S1P levels in the skin to regulate mechanical sensitivity and for increasing S1P under inflammatory/injury conditions to promote pain hypersensitivity.

Recent studies have identified distinct populations of AM nociceptors that are required for mechanical pain[5,6]. Likewise, it was discovered that a subset of somatostatin-expressing spinal interneurons is required for mechanical pain transduction[7]. Although these papers delineate the cells and circuitry of mechanical pain, the molecular underpinnings of mechanonociception in the periphery are poorly understood. While the identity of the transduction channel(s) in AM nociceptors remains enigmatic, understanding molecular mechanisms that regulate excitability will no doubt provide key insights into the function and specialization of the diverse subtypes of mechanosensitive nerve fibers. For example, although *Piezo2*-hypomorphic animals exhibit normal mechanical pain behaviors[3], *ex vivo* skin-nerve recordings show that their AM nociceptors display decreased force-responsiveness[3], and a recent study found that subpopulations of sensory neurons express different splice variants of *Piezo2* that exhibit different force sensitivities[45]. These studies suggest that mechanosensitive neurons exhibit functional specialization on multiple levels. Our study demonstrates that S1PR3 is indispensable for normal function of AM nociceptors, including the adapting AM population, recently discussed in Arcourt *et al.,* that innervates the epidermis and encodes noxious touch[5]. We show that S1PR3 signaling modulates KCNQ2/3 channels to regulate excitability of these A mechanonociceptors (**Figure 8**).

GPCR-mediated inhibition of KCNQ2/3 potassium channels is a well-known mechanism by which neuronal excitability is regulated[46]. Other studies have shown that KCNQ channels mediate excitability of Aδ fibers[30,31] and are required for normal mechanonociceptive responses in dorsal horn neurons receiving Aδ input[31], and that opening KCNQ2/3 channels directly with retigabine alleviates pain *in vivo*[33,47,48]. Our results not only complement previous work implicating KCNQ2/3 channels in pain, but also define the upstream mechanisms that promote the regulation of KCNQ2/3 channels to tune mechanical pain thresholds. Our data thus highlight S1PR3 as a novel and attractive target for the treatment of mechanical pain and describe a new signaling pathway by which S1P regulates AM nociceptor excitability.

Interestingly, the neurons that innervate the ultra-sensitive tactile organ of the star-nosed mole are highly enriched in transcripts for S1PR3 and KCNQ channels, as well as for a variety of other potassium channels[22]. While it is difficult to directly examine the physiological basis for heightened mechanosensitivity in the star-nosed mole, S1PR3-dependent modulation of KCNQ may represent an important mechanism underlying the high tactile sensitivity of the star organ. Moreover, link between *S1pr3* and *Kcnq2/3* are echoed in single-cell RNA seq datasets from mouse DRG neurons, which show co-expression of *S1pr3* and *Kcnq2/3* in a subset of myelinated mechanoreceptors[19]. These cells are distinct from the *S1pr3/Trpv1* subset that mediates S1P-evoked acute pain and heat hypersensitivity. In addition to being transcriptionally distinct, we show that the mechanisms underlying S1P's activities in these cells are functionally distinct. Finally, *S1pr3* and *Kcnq2/3* are highly expressed in human sensory ganglia[49,50] and recordings from human stem cell-derived sensory neurons show that KCNQ2/3 channels play a key role in mediating their excitability[51]. Thus S1PR3 signaling may represent a new target for modulating mechanical pain.

Previous studies of S1P signaling in DRG neurons focused on S1P-evoked excitation of small diameter and/or capsaicin-sensitive neurons, and pain behaviors triggered by elevated S1P. While our new data affirms the effects S1P in thermal nociceptors observed by others, our manuscript highlights a novel effect of baseline levels of S1P in modulation of rheobase and KCNQ2/3 currents in mechanonociceptors. We are also the first to examine the role of S1PR3 in a variety of somatosensory behaviors under normal

413 conditions (non-injury, no algogen injection), and to demonstrate a key role for S1PR3 in
414 mechanonociception. We also go beyond previous studies[12,13,16,17] in showing that elevated S1P
415 selectively promotes thermal and not mechanical hypersensitivity. Previous studies have shown that there
416 are distinct cells and molecular pathways that trigger thermal versus mechanical hypersensitivity. For
417 example, thermal hypersensitivity in CFA is dependent on TRPV1 ion channels[1] and independent of
418 immune cell infiltration[39]. By contrast, infiltration of a subset of myeloid immune cells is required for
419 mechanical hypersensitivity in an inflammatory pain model[39]. Here we show that S1P via S1PR3 signaling
420 is a key component of the inflammatory soup that triggers thermal hypersensitivity in the CFA model. Our
421 observation that S1PR3 KO animals display normal immune cell infiltration and develop mechanical
422 hypersensitivity after CFA is consistent with these previous studies showing distinct mechanisms of
423 inflammatory thermal and mechanical hypersensitivity.
424
425 Outside of the nervous system, S1P signaling via S1PR1 allows for the continuous circulation of
426 lymphocytes between blood, lymph, and peripheral tissues[9]. Our findings that S1P plays a key role in
427 noxious mechanosensation are in line with recent studies showing that sensory neurons co-opt classical
428 immune pathways to drive chronic itch or pain[52,53]. What distinguishes this study from the others is that S1P
429 signaling is critical for acute mechanical pain, even in the absence of inflammation or exogenously elevated
430 S1P. In the immune system, disruptions in S1P levels or S1PR1 signaling result in significant immune
431 dysfunction and disease[54–56]. Accordingly, in the somatosensory system, excessive, high levels of S1P
432 (micromolar), such as those present in inflammation, evokes thermal pain and sensitization. Intermediate,
433 baseline levels (nanomolar) regulate AM excitability and are required for normal mechanical pain
434 sensation. By contrast, lowering S1P levels reduces mechanical pain sensation, while sparing innocuous
435 touch sensation.
436
437 We propose that S1PR3 signaling may contribute to a variety of inflammatory diseases. S1P has been
438 linked to a wide range of human inflammatory disorders[57–63]. Canonically, S1P signaling via S1PR1 is
439 thought to promote inflammation via the immune system[58], however, we propose that S1P signaling via
440 S1PR3 in neurons may also contribute to inflammatory disease. Indeed, fingolimod, a non-selective S1PR

441 modulator, is prescribed as an immunosuppressant for multiple sclerosis treatment[14], but the possibility that
442 some of its therapeutic effects may also be mediated via the nervous system has not been fully explored.
443 Likewise, one study found that intrathecal fingolimod reduces bone cancer pain[64], and while analgesia was
444 attributed to effects on S1PR1 in glia, some of the benefits may be due to S1PR3 signaling in DRG
445 neurons. S1PR3 antagonism may also be useful in the treatment of inflammatory pain due to its selective
446 dampening of acute mechanical pain and inflammatory thermal hypersensitivity, while preserving
447 innocuous touch and normal thermal sensitivity. S1PR3 inhibitors may also be beneficial for treating other
448 inflammatory disorders where S1PR3-expressing somatosensory neurons have been shown to contribute
449 to neurogenic inflammation, such as asthma[65]. Our study demonstrates a crucial role for S1P signaling in
450 the peripheral nervous system and highlights the potential of S1PR3 as a target for future pain therapies.
451

452 Materials and Methods

453 *Behavioral studies & mice*

454 *S1pr3*$^{mcherry/+}$ and *S1pr3*$^{-/-}$ mice were obtained from Jackson Laboratory and backcrossed to C57bl6/J.
455 Wherever possible, wild-type/heterozygous (*S1pr3)* littermate controls were used in behavioral
456 experiments. Mice (20–25 g) were housed in 12 h light-dark cycle at 21°C. Mice were singly housed one
457 week prior to all behavioral experiments and were between 8-10 weeks at the time of the experiment. All
458 mice were acclimated in behavioral chambers (IITC Life Sciences) on 2 subsequent days for 1 hour prior to
459 all behavioral experiments.
460

461 Itch and acute pain behavioral measurements were performed as previously described[44,66,67]. Mice were
462 shaved one week prior to itch behavior. Compounds injected: 500 µM TY 52156 (Tocris), 50 µM SKI II
463 (Tocris), 0.2-10 µM S1P (Tocris, Avanti Polar Lipids), 50 mM chloroquine (Sigma), and 27 mM histamine
464 (Tocris) in PBS with either 0.01-0.1% Methanol- (S1P) or 0.1-0.5% DMSO-PBS (all other compounds)
465 vehicle controls. Pruritogens were injected using the cheek model (20 µL) of itch, as previously described[68].
466 Behavioral scoring was performed while blind to experimental condition and mouse genotype. All
467 scratching and wiping behavior videos were recorded for 1 hour. Itch behavior was scored for the first 30
468 minutes and acute pain was scored for the first five minutes. Bout number and length were recorded.

For radiant heat and von Frey hypersensitivity behavior, drugs were injected intradermally into the plantar surface of the hindpaw (20 µL). Radiant heat assays were performed using the IITC Life Science Hargreaves test system. Mechanical threshold was measured using calibrated von Frey monofilaments (Touch Test) on a metal grate platform (IITC). Von Frey was performed as previously described[67,69] using the up-down method[70] while blinded to compound injected and genotype, or a descending force-series of 4 trials per force from 0.4 g to 6 g. Valid responses for both von Frey and radiant heat included fast paw withdrawal, licking/biting/shaking of the affected paw, or flinching. For radiant heat and von Frey, mice were allowed to acclimate on platform for 1 hour before injection. Measurements were taken 15 minutes pre-injection and 20-30 minutes post-injection for all compounds used.

The pinprick assay[7] was conducted on a von Frey testing platform (IITC). The mouse hindpaw was poked with a 31 g syringe needle without breaking the skin to induce fast acute mechanical pain. Each paw was stimulated 10 times with the needle, with five minutes rest in between trials, and the % withdrawal (fast withdrawal, licking/biting/shaking of paw, squeaking, and/or flinching) was calculated from the total number of trials.

The tape assay was conducted according to previously described methods[3]. Number of attempts to remove a 3 cm piece of lab tape was recorded for 10 minutes after manual tape application to the rostral back. Scorer and experimenter were blinded to genotype.

For righting reflex measurements, age-matched *S1pr3*$^{-/-}$ and $^{+/+}$ P6-7 neonates were used. Briefly, pups were overturned one at a time on the home cage lid while experimenter was blinded to genotype. The time to righting was measured to the nearest 1/10th of a second with a stopwatch.

For the CFA model of hypersensitivity, mice were lightly anesthetized with isoflurane (2%) and injected with 15 µL CFA (Sigma) into one hindpaw using a Hamilton syringe (30 g) at 5pm. Radiant heat latencies and von Frey 50% withdrawal thresholds were recorded one day prior to CFA, the morning of CFA (prior to

injection), and one and two days post-CFA. Von Frey measurements were acquired before radiant heat latencies, and mice were allowed a one-hour recovery period in home cage with access to food and water in between testing. Both ipsilateral and contralateral paw were measured. Experimenter was blind to genotype for injections and recording.

All behavior experiments were carried out using age-matched or littermate cohorts of male mice and conducted between 8am and 1pm. Mice were tested in 4-part behavior chambers (IITC Life Sciences) with opaque dividers (TAP Plastics) with the exception of righting reflex measurements. Scratching and wiping behaviors were filmed from below using high-definition cameras. All experiments were performed under the policies and recommendations of the International Association for the Study of Pain and approved by the University of California, Berkeley Animal Care and Use Committee.

In situ hybridization (ISH)

Fresh DRG were dissected from 8-12 week old mice, flash frozen in OCT embedding medium, and sectioned at 14 µm onto slides. ISH was performed using Affymetrix Quantigene ViewISH Tissue 2-plex kit according to manufacturer's instructions with Type 1 (*S1pr3*) and Type 6 (all other) probes. The following probes against mouse mRNAs were created by Affymetrix and used for ISH: *S1pr3, Scn1a, Npy2r, Piezo2, Trpv1, Trpa1.*

Immunohistochemistry (IHC) of DRG

DRG were dissected from 8-12 week old adult mice and post-fixed in 4% PFA for one hour. DRG were cryo-protected overnight at 4°C in 30% sucrose-PBS, embedded in OCT, and then cryosectioned at 12 µm onto slides. Briefly, slides were washed 3x in PBST (0.3% Triton X-100), blocked in 2.5% horse serum + 2.5% BSA PBST, and incubated overnight at 4°C in 1:1000 primary antibody in PBST + 0.5% horse serum + 0.5% BSA. Slides were washed 3X in PBS then incubated 1-2 hours at RT in 1:1000 secondary antibody. Slides were washed 3X in PBS and mounted in Fluoromount-G + DAPI with No. 1.5 coverglass. Primary antibodies used: Rabbit anti-DsRed (Clontech #632496), Rabbit anti-S1PR3 (Abcam #38324; #108370), Mouse anti-NF200 (Sigma #N5389), Chicken anti-Peripherin (Abcam #39374). Secondary antibodies used:

Goat anti-Mouse Alexa 488 (Abcam #150117), Goat anti-Chicken Alexa 488 (ThermoFisher #A11039), Goat anti-Rabbit Alexa 594 (Invitrogen #R37117). Isolectin B4 (IB4)-FITC (Enzo Life Sciences #ALX-650-001F-MC05) was also used. Slides were mounted in Fluoromount with No. 1.5 coverglass. Imaging of DRG ISH and IHC experiments, and all live-cell imaging, was performed on an Olympus IX71 microscope with a Lambda LS-xl light source (Sutter Instruments). For DRG ISH and IHC analysis, images were analyzed using FIJI software. Briefly, DAPI-positive cells were circled and their fluorescence intensity (AFU) for all channels was plotted against cell size using Microsoft Excel software. Co-labeling analysis was performed using FIJI. Intensity thresholds were set based on the negative control (no probe) slide. Cells were defined as co-expressing if their maximum intensities exceeded the threshold for both channels of interest.

IHC of sectioned skin

Skin was dissected from 8 week old adult mice and post-fixed in 4% PFA for 30 minutes at RT. DRG were cryo-protected overnight at 4°C in 30% sucrose-PBS, embedded in OCT, and then sectioned at 18 µm onto slides. Briefly, slides were blocked in 5% normal goat serum in PBST (0.1% Triton X-100) and incubated overnight at 4°C in 1:1000 primary antibody in blocking buffer. Slides were washed 3X in PBS then incubated 45 minutes at RT in 1:1000 secondary antibody. Slides were washed 5X in PBS and mounted in Fluoromount-G + DAPI with No. 1.5 coverglass. Primary antibodies used: Rabbit anti-DsRed (Clontech #632496), Chicken anti-NefH (Abcam #4680), Chicken anti-β-tubulin III (Abcam #107216), mouse anti-PGP9.5 (Abcam #8189). Secondary antibodies used: Goat anti-Mouse Alexa 488 (Abcam #150117), Goat anti-Rabbit Alexa 594 (Invitrogen #R37117), Goat anti-Chicken Alexa 488 (ThermoFisher #A11039). For co-localization analysis, only fibers for which > 50% of the length of the visible fiber contained co-localized (white) pixels were counted. Image analysis was performed using FIJI.

Whole mount skin IHC

Staining was performed according to Marshall and Clary *et al*[71]. Briefly, 8-week-old mice were euthanized and the back skin was shaved, depilated, and tape-stripped. The removed skin was fixed overnight in 4% PFA, then washed in PBS (3X for 10 minutes each). Dermal fat was scraped away with a scalpel and skin was washed in PBST (0.3% Triton X-100; 3X for two hours each) then incubated in 1:500 primary antibody

(Rabbit anti DsRed: Clontech #632496; Chicken anti-Nefh: Abcam #4680) in blocking buffer (PBST with 5% goat serum and 20% DMSO) for 5.5 days at 4°C. Skin was washed as before and incubated in 1:500 secondary antibody (Goat anti-Rabbit Alexa 594; Invitrogen #R37117; Goat anti-Chicken Alexa 488; ThermoFisher #A11039) in blocking buffer for 3 days at 4°C. Skin was washed in PBST, serially dried in methanol: PBS solutions, incubated overnight in 100% methanol, and finally cleared with a 1:2 solution of benzyl alcohol: benzyl benzoate (BABB; Sigma) before mounting between No. 1.5 coverglass. Sectioned and whole mount skin samples were imaged on a Zeiss LSM 880 confocal microscope with OPO using a 20x water objective. Image analysis was performed using FIJI.

Cell culture

Cell culture was carried out as previously described[72]. Briefly, neurons from dorsal root ganglia (2-8 week old adults) or trigeminal ganglia (P0) were dissected and incubated for 10 min in 1.4 mg ml−1 Collagenase P (Roche) in Hanks calcium-free balanced salt solution, followed by incubation in 0.25% standard trypsin (vol/vol) STV versene-EDTA solution for 2 min with gentle agitation. Cells were then triturated, plated onto Poly D-Lysine coated glass coverslips and used within 20 h. Media: MEM Eagle's with Earle's BSS medium, supplemented with 10% horse serum (vol/vol), MEM vitamins, penicillin/streptomycin and L-glutamine.

Calcium imaging

Ca^{2+} imaging experiments were carried out as previously described[72]. Cells were loaded for 60 min at room temperature with 10 µM Fura-2AM supplemented with 0.01% Pluronic F-127 (wt/vol, Life Technologies) in a physiological Ringer's solution containing (in mM) 140 NaCl, 5 KCl, 10 HEPES, 2 CaCl2, 2 MgCl2 and 10 D-(+)-glucose, pH 7.4. All chemicals were purchased from Sigma. Acquired images were displayed as the ratio of 340 nm/ 380 nm. Cells were identified as neurons by eliciting depolarization with high potassium Ringer's solution (75 mM) at the end of each experiment. Responding neurons were defined as those having a > 15% increase from baseline ratio. Image analysis and statistics were performed using automated routines in Igor Pro (WaveMetrics). Fura-2 ratios were normalized to the baseline ratio F340/F380 = (Ratio)/(Ratio t = 0).

581

582 *In vitro electrophysiology*

583 Electrophysiological experiments were carried out as previously described[72]. Briefly, recordings were
584 collected at 5 kHz and filtered at 2 kHz (Axopatch 200B, pClamp software). Electrode resistance ranged
585 between 1.5–5 MΩ. Internal solution contained 140 mM KCl, 2 mM MgCl2, 1 mM EGTA, 5 mM HEPES, 1
586 mM Na2ATP, 100 μM GTP, and 100 μM cAMP (pH 7.4). Bath solution was physiological Ringer's solution.
587 The pipette potential was canceled before seal formation. Cell capacitance was canceled before whole cell
588 voltage-clamp recordings. For mechanonociceptors experiments, only cells which were visually identified
589 as mCherry expressing and which had a capacitance between 40-80 pF were used. Rheobase was
590 calculated as the smallest current step required to elicit an action potential using current steps of 50 pA. M
591 currents were measured and analyzed using standard protocols for DRG neurons reported in the
592 literature[30,32,73]. Experiments were carried out only on cells with a series resistance of less than 30
593 MΩ. Analysis of electrophysiology data was performed in pClamp and IgorPro.

594

595 *Ex vivo skin-nerve electrophysiology*

596 Touch-evoked responses in the skin were recorded after dissecting the hind limb skin and saphenous
597 nerve from 7-10 week old mice, according to published methods[74,75]. The skin was placed epidermis-side-
598 up in a custom chamber and perfused with carbogen-buffered synthetic interstitial fluid (SIF) kept at 32 °C
599 with a temperature controller (model TC-344B, Warner Instruments). The nerve was kept in mineral oil in a
600 recording chamber, teased apart, and placed onto a gold recording electrode connected with a reference
601 electrode to a differential amplifier (model 1800, A-M Systems). The extracellular signal was digitized using
602 a PowerLab 8/35 board (AD Instruments) and recorded using LabChart software (AD Instruments).

603

604 For these studies, we focused on A-mechanonociceptors (AMs). To identify responses from these afferents
605 in mutant and control genotypes, we used a mechanical search paradigm with a fine glass probe. Afferents
606 were classified as AMs according to the following criteria: (1) conduction velocity (approximately, 1 to (≤ 12
607 m/s^{-1}), (2) medium-sized receptive fields, (3) sustained response to mechanical indentation[74,76,77].

608

609 Touch-sensitive afferents that did not meet these criteria were not analyzed further. Responses were
610 classified as Adapting AMs if the ratio of mean firing rate in the dynamic phase of stimulation (first 0.2 s) to
611 the static phase of stimulation (last 4.8 s) was greater than 2, and Non-Adapting AMs if the ratio was less
612 than or equal to 2. Non-responders (**Figure 6F**) responded to suprathreshold mechanical stimulation with
613 von Frey monofilaments (tip diameter <0.5 mm), but not to maximal controlled mechanical stimulation (256
614 mN, tip diameter 2 mm). All recordings and analyses were performed blind to genotype.
615
616 Mechanical responses were elicited with von Frey monofilaments and a force controlled custom-built
617 mechanical stimulator. Mechanical thresholds were defined as the lowest von Frey monofilament to reliable
618 elicit at least on action potential. Force controlled mechanical stimuli were delivered using a computer
619 controlled, closed-loop, mechanical stimulator (Model 300C-I, Aurora Scientific, 2 mm tip diameter). Low-
620 pass filtered, 5-second long, length control steps (square wave) simultaneously delivered with permissive
621 force control steps (square wave) were generated using LabChart software (AD Instruments). An arbitrarily
622 selected force step-and-hold protocol (8, 32, 4, 64, 128, 16, 256 mN) was delivered to all fibers. The period
623 between successive displacements was 60 seconds.
624
625 Conduction velocity was measured by electrically stimulating identified receptive fields. Spike sorting by
626 principal component analysis (PCA) and density based clustering, and data analysis was performed off-line
627 with custom-made software in MATLAB. Statistics were performed in Prism.
628
629 *Flow cytometry of CFA-treated hind paws*
630 CFA injections were performed as described above. Briefly, hindpaw skin and underlying fascia of treated
631 and PBS-injected paws were removed from freshly euthanized mice. Skin was placed in RPMI media
632 (Gibco) on ice before mincing with dissection scissors. Digestions were performed for 90 minutes at 37°C
633 on a rotating platform in 1 mL RPMI supplemented with 1:1000 DNaseI enzyme (Roche) and 1 unit
634 LiberaseTM (Roche). Skin was then filtered through 70 µm nylon mesh (Falcon), washed in RPMI, and
635 resuspended in PBS for Aqua Live-Dead staining. Samples were then transferred to FACS buffer (PBS
636 with 0.5% FBS and 2 mM EDTA), blocked, then surface stained with the following antibodies: cKit-Biotin,

FceRI-PE, CD49b-PECy7, SiglecF-APC, SA-FITC, Ly6C-PerCP, CD11b-PB, Ly6G-BV785, CD45.2-AF700. Compensation tubes (single-stain) were prepared for each fluorophore using positive and negative control beads. A spleen from a wild-type animal was also prepared by crushing between frosted glass slides, straining through 70 µm nylon mesh, and lysing of erythrocytes in ACK (Gibco). A portion of spleen sample was heat-killed for 10 minutes at 65°C and stained with Aqua viability stain and set aside. The rest of the spleen was stained normally with the other skin samples. Samples were then run through a flow cytometer (BD Fortessa). Data were analyzed using FlowJo (Prism) and Microsoft Excel. Neutrophils were defined as live single cells with the following staining profile: $CD45.2^+/CD11b^+/Ly6G^+/Ly6C^+$. Inflammatory monocytes were defined as the following: $CD45.2^+/CD11b^+/Ly6G^-/Ly6C^{high}$. Total number of immune cells was reported, rather than percentage of total, since neither genotype differed significantly in total number of live cells or total number of $CD45.2^+$ immune cells.

Statistical analyses

All statistical analyses, except for skin nerve data (see above), were performed using IgorPro software or Microsoft Excel. Values are reported as the mean ± SEM where multiple independent experiments are pooled and reported (for whole cell electrophysiology), and mean ± SD where one experiment was performed with multiple wells (for calcium imaging) or mice (for behavior). For comparison between two groups, Student's unpaired 2-tailed t-test was used. A paired t-test was employed only for measurements within the same biological replicate and after a given treatment. For single-point comparison between >2 groups, a one-way ANOVA followed by appropriate post hoc test was used, depending on comparison. For the time course comparison between 2 groups, 2-way ANOVA was used and single comparison p-values were derived using Tukey's HSD or appropriate statistical test, depending on comparison. Number of mice or samples required to attain significance was not calculated beforehand, and where multiple statistical tests were performed, a Bonferroni correction was applied. In figure legends, significance was labeled as: n.s., not significant, $p \geq 0.05$; *$p < 0.05$; **$p < 0.01$; ***$p < 0.001$.

Key Resources Table				
Reagent type (species) or resource	**Designation**	**Source or reference**	**Identifiers**	**Additional information**
strain, strain background(C57BL/6J)	C57BL/6J; WT; wild-type	The Jackson Laboratory	Jackson Stock #: 000664; RRID:IMSR_JAX:000664	
strain, strain background(B6.129S6-S1pr3tm1Rlp/Mmnc)	S1PR3 KO; S1pr3-/-	MMRRC Repository; https://www.ncbi.nlm.nih.gov/pubmed/15138255; PMID: 15138255	B6.129S6-S1pr3tm1Rlp/Mmnc; MMRRC Stock #: 012038-UNC; RRID:MMRRC_012038-UNC	
strain, strain background(B6.Cg-S1pr3tm1.1Hrose/J)	*S1pr3-mCherry; S1pr3mcherry/+*	The Jackson Laboratory	B6.Cg-S1pr3tm1.1Hrose/J; Jackson Stock #: 028624; RRID:IMSR_JAX:028624	
antibody(Living Colors DsRed Rabbit Polyclonal Antibody)	Rabbit anti-DsRed	Clontech	RRID:AB_10013483; Cat # 632496	
antibody(Chicken polyclonal to Neurofilament heavy polypeptide)	Chicken anti-NefH	Abcam	RRID:AB_304560; Cat # ab4680	
antibody(Chicken polyclonal to beta III Tubulin)	Chicken anti-β-tubulin III	Abcam	RRID:AB_10899689; Cat # ab107216	
antibody(Mouse monoclonal [13C4 / I3C4] to PGP9.5)	Mouse anti-PGP9.5	Abcam	RRID:AB_306343; Cat # ab8189	
antibody(Rabbit polyclonal to EDG3)	Rabbit anti-S1PR3	Abcam	RRID:AB_732070; Cat # ab38324	
antibody(Mouse monoclonal to NF200)	Mouse anti-NF200	Sigma-Aldrich	RRID:AB_260781; Cat # N5389	
antibody(Chicken polyclonal to Peripherin)	Chicken anti-Peripherin	Abcam	RRID:AB_777207; Cat # ab39374	
antibody(Goat Anti-Mouse IgG H&L Alexa Fluor 488)	Goat anti-Mouse Alexa 488	Abcam	RRID:AB_2688012; Cat # ab150117	
antibody(Goat anti-Chicken IgY (H+L) Secondary Antibody, Alexa Fluor 488)	Goat anti-Chicken Alexa 488	ThermoFisher Scientific	RRID:AB_2534096; Cat # A-11039	
antibody(Goat anti-Rabbit IgG (H+L) Secondary Antibody, Alexa Fluor 594)	Goat anti-Rabbit Alexa 594	Invitrogen	RRID:AB_2556545; Cat # R37117	
sequence-based reagent	*S1pr3* Type I Probe	ThermoFisher Scientific; Affymetrix	Assay ID: VB1-19668-VC	
sequence-based reagent	*Scn1a* Type 6 Probe	ThermoFisher Scientific; Affymetrix	Assay ID: VB6-18173-VC	

sequence-based reagent	*Npy2r* Type 6 Probe	ThermoFisher Scientific; Affymetrix	Assay ID: VB6-3197254-VC	
sequence-based reagent	*Piezo2* Type 6 Probe	ThermoFisher Scientific; Affymetrix	Assay ID: VB6-18046-VC	
sequence-based reagent	*Trpv1* Type 6 Probe	ThermoFisher Scientific; Affymetrix	Assay ID: VB6-18246-VC	
sequence-based reagent	*Trpa1* Type 6 Probe	ThermoFisher Scientific; Affymetrix	Assay ID: VB6-16610-VC	
commercial assay or kit(ViewRNA ISH Tissue Assay Kit (2-plex))	ViewRNA ISH Tissue Assay Kit	ThermoFisher Scientific; Affymetrix	Cat # QVT0012	
chemical compound, drug(Sphingosine-1-phosphate)	Sphingosine 1-phosphate; S1P	Tocris Bioscience; Avanti Polar Lipids	CAS 26993-30-6; Cat # 1370; Cat # 860641	
chemical compound, drug(TY 521256)	TY 52156	Tocris Bioscience	CAS 934369-14-9; Cat # 5328	
chemical compound, drug(SKI II)	SKI II	Tocris Bioscience	CAS 312636-16-1; Cat # 2097	
chemical compound, drug(Histamine dihydrochloride)	Histamine	Sigma-Aldrich	CAS 56-92-8; Cat # H7250	
chemical compound, drug(Chloroquine diphosphate)	Chloroquine	Sigma-Aldrich	CAS 50-63-5; Cat # C6628	
chemical compound, drug(E-Capsaicin)	Capsaicin	Tocris Bioscience	CAS 404-86-4; Cat # 0462	
chemical compound, drug(Dimethyl sulfoxide)	DMSO	Sigma-Aldrich	Cat # 8418-100mL	
chemical compound, drug(Methanol)	Methanol	Sigma-Aldrich	CAS 67-56-1; Cat # 34860	
chemical compound, drug(Linopirdine dihydrochloride)	Linopirdine	Tocris Bioscience	CAS 113168-57-3; Cat # 1999	
chemical compound, drug(XE 991 dihydrochloride)	XE 991	Tocris Bioscience	CAS 122955-13-9; Cat # 2000	
chemical compound, drug(W146)	W146	Tocris Bioscience	CAS 909725-61-7; Cat # 3602	
chemical compound, drug(Freund's Adjuvant, Complete)	Complete Freund's Adjuvant; CFA	Sigma-Aldrich	Cat # F5881	
chemical compound, drug(Formaldehyde, 16%, methanol	Paraformaldehyde; PFA	Polysciences, Inc.	Cat # 18814-10	

free, Ultra Pure)				
chemical compound, drug(Tissue Tek Optimal cutting temperature compound (OCT))	OCT	Sakura Finetek USA	Cat # 4583	
chemical compound, drug(Triton X-100 solution)	Triton X-100	BioUltra	CAS 9002-93-1; Cat # 93443	
chemical compound, drug(Phosphate-buffered saline (PBS), pH 7.4)	PBS	Gibco	Cat # 10010023	
chemical compound, drug(Benzyl benzoate)	Benzyl benzoate	Sigma-Aldrich	CAS 120-51-4; Cat # B6630	
chemical compound, drug(Benzyl alcohol)	Benzyl alcohol	Sigma-Aldrich	CAS 100-51-6; Cat # 305197	
chemical compound, drug(Sucrose)	Sucrose	Sigma-Aldrich	CAS 57-50-1; Cat # S0389	
chemical compound, drug(LIVE/DEAD Fixable Aqua Dead Cell Stain Kit, for 405 nm excitation)	Aqua	ThermoFisher Scientific	Cat # L34957	
chemical compound, drug(Isoflurane, USP)	Isoflurane	Piramal	CAS 26675-46-7	
chemical compound, drug(4',6-Diamidino-2-Phenylindole, Dihydrochloride)	DAPI	ThermoFisher Scientific	CAS 28718-90-3; Cat # 1306	
chemical compound, drug(Fluoromount-G, with DAPI)	Fluoromount-G, with DAPI	ThermoFisher Scientific	Cat # 00-4959-52	
antibody(CD117 (c-Kit) Monoclonal Antibody (2B8), Biotin)	c-Kit-Biotin	eBioscience	RRID:AB_466569; Cat # 13-1171-82	
antibody(FceR1 alpha Monoclonal Antibody (AER-37 (CRA1)), PE, eBioscience)	FceRI-PE	eBioscience	RRID:AB_10804885; Cat # 12-5899-42	
antibody(CD49b (Integrin alpha 2) Monoclonal Antibody (DX5), PE-Cyanine7, eBioscience)	CD49b-PECy7	eBioscience	RRID:AB_469667; Cat # 25-5971-82	

antibody(Anti-Siglec-F-APC, mouse (clone: REA798))	SiglecF-APC	Miltenyi Biotech	RRID:AB_2653441; Cat # 130-112-333	
antibody(Streptavidin FITC)	SA-FITC	eBioscience	RRID:AB_11431787; Cat # 11-4317-87	
antibody(Ly-6C Monoclonal Antibody (HK1.4), PerCP-Cyanine5.5, eBioscience)	Ly6C-PerCP	eBioscience	RRID:AB_1518762; Cat # 45-5932-82	
antibody(Pacific Blue anti-mouse/human CD11b Antibody)	CD11b-PB	BioLegend	RRID:AB_755985; Cat # 101223	
antibody(Brilliant Violet 785 anti-mouse Ly-6G Antibody)	Ly6G-BV785	BioLegend	RRID:AB_2566317; Cat # 127645	
antibody(CD45.2 Monoclonal Antibody (104), Alexa Fluor 700, eBioscience)	CD45.2-AF700	eBioscience	RRID:AB_657752; Cat # 56-0454-82	
software, algorithm(Igor Pro version 6.3)	IgorPro	WaveMetrics	https://www.wavemetrics.com/order/order_igordownloads6.htm	
software, algorithm(Microsoft Excel 2011)	Microsoft Excel	Microsoft	https://www.microsoft.com/en-us/store/d/excel-2016-for-mac/	
software, algorithm(pClamp 10)	pClamp	Axon	http://mdc.custhelp.com/app/answers/detail/a_id/18779/~/axon%E2%84%A2-pclamp%E2%84%A2-10-electrophysiology-data-acquisition-%26-analysis-software	
software, algorithm(MetaFluor 7.8)	MetaFluor	Molecular Devices	https://www.moleculardevices.com/systems/metamorph-research-imaging/metafluor-fluorescence-ratio-imaging-software	
software, algorithm(MATLAB)	MATLAB	MathWorks	https://www.mathworks.com/downloads/	
software, algorithm(FIJI)	FIJI	NIH	https://imagej.net/Fiji/Downloads	
software, algorithm(LabChart Software)	LabChart Software	AD Instruments	https://www.adinstruments.com/products/labchart	
software, algorithm(Graphpad Prism 7)	Graphpad Prism	Graphpad	https://www.graphpad.com/scientific-software/prism/	
software, algorithm(FlowJo 10.4.2)	FlowJo	FlowJo	https://www.flowjo.com/solutions/flowjo/downloads	
software, algorithm(custom)	custom-made software in MATLAB	this paper	NA	www.GitHub.com/buh2003/SpikeSortingPCA_DBSCAN

other(Bovine serum albumin, cold ethanol fraction, pH 5.2, ≥96%)	BSA	Sigma-Aldrich	CAS 9048-46-8; Cat # A4503	
other(Isolectin B4 (Bandeireia simplicifolia), FITC-conjugate)	IB4-FITC; IB4	Enzo Life Sciences	Cat # ALX-650-001F-MC05	
other(Normal Goat Serum)	NGS	Abcam	Cat # ab7481	
peptide, recombinant protein(δ-theraphototoxin-Hm1a)	Hm1a	other; https://www.ncbi.nlm.nih.gov/pmc/articles/PMC4919188/; PMID: 4919188	NA	obtained from the laboratory of David Julius (UCSF)

Acknowledgements

We thank Z. Rifi (UC Berkeley) for assistance with scoring itch behavior, R. P. Dalton (UC Berkeley) for assistance with confocal microscopy, and P. Lishko and M. Miller (UC Berkeley) for advice on lipid stability and usage. We would also like to thank R. Clary (Columbia) for whole mount skin staining protocols, B. Jenkins (Columbia) for advice on the immunohistochemistry experiments, and D. Julius (UC San Francisco) for the gift of Hm1a spider toxin. Confocal imaging experiments were conducted at the CRL Molecular Imaging Center, supported by the Helen Wills Neuroscience Institute (UC Berkeley). We would like to thank H. Aaron and J. Lee for their microscopy training and assistance. We are grateful to all members of the D.M.B Laboratory (UC Berkeley) for constructive feedback and criticism. The National Institutes of Health grants NS077224 and NS098097 (to D.M.B and R.B.), AR059385 (to D.M.B.), AR051219 (to E.A.L), NS105449 and GM007367 (to B.U.H), and NS063307 (to the Neurobiology Course at the Marine Biological Laboratory); and a Howard Hughes Medical Institute Faculty Scholars grant (to D.M.B) supported this work.

Competing interests

The authors declare no competing interests at this time.

References

1. Caterina, M. J. *et al.* Impaired Nociception and Pain Sensation in Mice Lacking the Capsaicin

685 Receptor. *Science.* **288,** 306–313 (2000).
686 2. Vriens, J. *et al.* TRPM3 Is a Nociceptor Channel Involved in the Detection of Noxious Heat. *Neuron*
687 **70,** 482–494 (2011).
688 3. Ranade, S. S. *et al.* Piezo2 is the major transducer of mechanical forces for touch sensation in mice.
689 *Nature* **516,** 121–125 (2014).
690 4. Woo, S.H. *et al.* Piezo2 is required for Merkel-cell mechanotransduction. *Nature* **509,** 622–626
691 (2014).
692 5. Arcourt, A. *et al.* Touch Receptor-Derived Sensory Information Alleviates Acute Pain Signaling and
693 Fine-Tunes Nociceptive Reflex Coordination. *Neuron* **93,** 179–193 (2017).
694 6. Ghitani, N. *et al.* Specialized Mechanosensory Nociceptors Mediating Rapid Responses to Hair Pull.
695 *Neuron* **95,** 944–954.e4 (2017).
696 7. Duan, B. *et al.* Identification of Spinal Circuits Transmitting and Gating Mechanical Pain. *Cell* **159,**
697 1417–1432 (2014).
698 8. Spiegel, S. & Milstien, S. Sphingosine-1-phosphate: an enigmatic signalling lipid. *Nat Rev Mol Cell*
699 *Biol* **4,** 397–407 (2003).
700 9. Matloubian, M. *et al.* Lymphocyte egress from thymus and peripheral lymphoid organs is dependent
701 on S1P receptor 1. *Nature* **427,** 355–360 (2004).
702 10. Schwab, S. R. *et al.* Lymphocyte sequestration through S1P lyase inhibition and disruption of S1P
703 gradients. *Science* **309,** 1735–1739 (2005).
704 11. Janes, K. *et al.* The development and maintenance of paclitaxel-induced neuropathic pain require
705 activation of the sphingosine 1-phosphate receptor subtype 1. *J. Biol. Chem.* **289,** 21082–21097
706 (2014).
707 12. Mair, N. *et al.* Genetic evidence for involvement of neuronally expressed S1P1 receptor in nociceptor
708 sensitization and inflammatory pain. *PLoS One* **6,** (2011).
709 13. Camprubi-Robles, M. *et al.* Sphingosine-1-phosphate-induced nociceptor excitation and ongoing
710 pain behavior in mice and humans is largely mediated by S1P3 receptor. *J Neurosci* **33,** 2582–2592
711 (2013).
712 14. Brinkmann, V. *et al.* Fingolimod (FTY720): discovery and development of an oral drug to treat

713 multiple sclerosis. *Nat Rev Drug Discov* **9,** 883–897 (2010).
714 15. Couttas, T. a *et al.* Loss of the neuroprotective factor Sphingosine 1-phosphate early in Alzheimer's
715 disease pathogenesis. *Acta Neuropathol. Commun.* **2,** 9 (2014).
716 16. Finley, A. *et al.* Sphingosine 1-phosphate mediates hyperalgesia via a neutrophil-dependent
717 mechanism. *PLoS One* **8,** e55255 (2013).
718 17. Weth, D. *et al.* Activated platelets release sphingosine 1-phosphate and induce hypersensitivity to
719 noxious heat stimuli in vivo. *Front. Neurosci.* **9,** 1–8 (2015).
720 18. Weth-Malsch, D. *et al.* Ablation of Sphingosine 1-Phosphate Receptor Subtype 3 Impairs
721 Hippocampal Neuron Excitability In vitro and Spatial Working Memory In vivo. *Front. Cell. Neurosci.*
722 **10,** 1–12 (2016).
723 19. Usoskin, D. *et al.* Unbiased classification of sensory neuron types by large-scale single-cell RNA
724 sequencing. *Nat. Neurosci.* **18,** 145–153 (2015).
725 20. Zhang, Y. H., Fehrenbacher, J. C., Vasko, M. R. & Nicol, G. D. Sphingosine-1-phosphate via
726 activation of a G-protein-coupled receptor(s) enhances the excitability of rat sensory neurons. *J.*
727 *Neurophysiol.* **96,** 1042–1052 (2006).
728 21. Li, C., Li, J., Kays, J., Guerrero, M. & Nicol, G. D. Sphingosine 1-phosphate enhances the excitability
729 of rat sensory neurons through activation of sphingosine 1-phosphate receptors 1 and/or 3. *J.*
730 *Neuroinflammation* **12,** 1–20 (2015).
731 22. Gerhold, K. *et al.* The Star-Nosed Mole Reveals Clues to the Molecular Basis of Mammalian Touch.
732 *PLoS One* **8,** (2013).
733 23. Kono, M. *et al.* The sphingosine-1-phosphate receptors S1P1, S1P2, and S1P3 function coordinately
734 during embryonic angiogenesis. *J. Biol. Chem.* **279,** 29367–29373 (2004).
735 24. Nussbaum, C. *et al.* Sphingosine-1-phosphate receptor 3 promotes leukocyte rolling by mobilizing
736 endothelial P-selectin. *Nat. Commun.* **6,** 6416 (2015).
737 25. Chiba, Y., Takeuchi, H., Sakai, H. & Misawa, M. SKI-II, an inhibitor of sphingosine kinase,
738 ameliorates antigen-induced bronchial smooth muscle hyperresponsiveness, but not airway
739 inflammation, in mice. *J. Pharmacol. Sci.* **114,** 304–310 (2010).
740 26. Shaner, R. L. *et al.* Quantitative analysis of sphingolipids for lipidomics using triple quadrupole and

741 quadrupole linear ion trap mass spectrometers. *J. Lipid Res.* **50,** 1692–1707 (2009).
742 27. Sanna, M. *et al.* Bitopic S1P3 Antagonist Rescue from Complete Heart Block: Pharmacological and
743 Genetic Evidence for Direct S1P3 Regulation of Mouse Cardiac Conduction. *Mol. Pharmacol.* **89,**
744 176–186 (2015).
745 28. Osteen, J. D. *et al.* Selective spider toxins reveal a role for the Nav1.1 channel in mechanical pain.
746 *Nature* **534,** 494–9 (2016).
747 29. Joost, S. *et al.* Single-Cell Transcriptomics Reveals that Differentiation and Spatial Signatures
748 Shape Epidermal and Hair Follicle Heterogeneity. *Cell Syst.* **3,** 221–237.e9 (2016).
749 30. Schutze, S., Orozco, I. J. & Jentsch, T. J. KCNQ Potassium Channels Modulate Sensitivity of Skin
750 Down hair (D-hair) Mechanoreceptors. *J. Biol. Chem.* **291,** 5566–5575 (2016).
751 31. Passmore, G. M. *et al.* Functional significance of M-type potassium channels in nociceptive
752 cutaneous sensory endings. *Front. Mol. Neurosci.* **5,** 1–12 (2012).
753 32. Crozier, R. A., Ajit, S. K., Kaftan, E. J. & Pausch, M. H. MrgD Activation Inhibits KCNQ / M-Currents
754 and Contributes to Enhanced Neuronal Excitability. *J Neurosci* **27,** 4492–4496 (2007).
755 33. Xu, W. *et al.* Activation of Voltage-Gated KCNQ/Kv7 Channels by Anticonvulsant Retigabine
756 Attenuates Mechanical Allodynia of Inflammatory Temporomandibular Joint in Rats. *Mol. Pain* **6,**
757 1744-8069-6–49 (2010).
758 34. Ramos-Perez, W. D., Fang, V., Escalante-Alcalde, D., Cammer, M. & Schwab, S. R. A map of the
759 distribution of sphingosine 1-phosphate in the spleen. *Nat. Immunol.* **16,** 1245–52 (2015).
760 35. McIlwrath, S. L., Lawson, J. J., Anderson, C. E., Albers, K. M. & Koerber, H. R. Overexpression of
761 neurotrophin-3 enhances the mechanical response properties of slowly adapting type 1 afferents
762 and myelinated nociceptors. *Eur. J. Neurosci.* **26,** 1801–1812 (2007).
763 36. Kwan, K. Y., Glazer, J. M., Corey, D. P., Rice, F. L. & Stucky, C. L. TRPA1 Modulates
764 Mechanotransduction in Cutaneous Sensory Neurons. *J. Neurosci.* **29,** 4808–4819 (2009).
765 37. Smith, A. K., O'Hara, C. L. & Stucky, C. L. Mechanical sensitization of cutaneous sensory fibers in
766 the spared nerve injury mouse model. *Mol. Pain* **9,** 1–6 (2013).
767 38. Garrison, S. R., Dietrich, A. & Stucky, C. L. TRPC1 contributes to light-touch sensation and
768 mechanical responses in low-threshold cutaneous sensory neurons. *J. Neurophysiol.* **107,** 913–922

(2012).

39. Ghasemlou, N., Chiu, I. M., Julien, J.-P. & Woolf, C. J. CD11b $^{+}$ Ly6G $^{-}$ myeloid cells mediate mechanical inflammatory pain hypersensitivity. *Proc. Natl. Acad. Sci.* 201501372 (2015). doi:10.1073/pnas.1501372112

40. Abrahamsen, B. *et al.* The Cell and Molecular Basis of Mechanical, Cold, and Inflamatory Pain. *Science.* **321,** 702 (2008).

41. Lennertz, R. C., Kossyreva, E. A., Smith, A. K. & Stucky, C. L. TRPA1 mediates mechanical sensitization in nociceptors during inflammation. *PLoS One* **7,** 1–11 (2012).

42. Chalfant, C. E. & Spiegel, S. Sphingosine 1-phosphate and ceramide 1-phosphate: expanding roles in cell signaling. *J. Cell Sci.* **118,** 4605–4612 (2005).

43. Pappu, R. *et al.* Promotion of lymphocyte egress into blood and lymph by distinct sources of sphingosine-1-phosphate. *Science* **316,** 295–298 (2007).

44. Morita, T. *et al.* HTR7 Mediates Serotonergic Acute and Chronic Itch. *Neuron* **87,** 124–138 (2015).

45. Szczot, M. *et al.* Cell-Type-Specific Splicing of Piezo2 Regulates Mechanotransduction. *Cell Rep.* **21,** 2760–2771 (2017).

46. Passmore, G. M. *et al.* KCNQ/M currents in sensory neurons: significance for pain therapy. *J. Neurosci.* **23,** 7227–7236 (2003).

47. Hayashi, H., Iwata, M., Tsuchimori, N. & Matsumoto, T. Activation of peripheral KCNQ channels attenuates inflammatory pain. *Mol. Pain* **10,** 15 (2014).

48. Blackburn-Munro, G. & Jensen, B. S. The anticonvulsant retigabine attenuates nociceptive behaviours in rat models of persistent and neuropathic pain. *Eur. J. Pharmacol.* **460,** 109–116 (2003).

49. Ray, P. *et al.* Comparative transcriptome profiling of the human and mouse dorsal root ganglia: An RNA-seq-based resource for pain and sensory neuroscience research. *bioRxiv* 165431 (2017). doi:10.1101/165431

50. Flegel, C. *et al.* RNA-Seq analysis of human trigeminal and dorsal root ganglia with a focus on chemoreceptors. *PLoS One* **10,** 1–30 (2015).

51. Young, G. T. *et al.* Characterizing human stem cell-derived sensory neurons at the single-cell level

797 reveals their ion channel expression and utility in pain research. *Mol. Ther.* **22,** 1530–1543 (2014).
798 52. Oetjen, L. K. *et al.* Sensory Neurons Co-opt Classical Immune Signaling Pathways to Mediate
799 Chronic Itch. *Cell* **129,** 742–751 (2017).
800 53. Pinho-Ribeiro, F. A., Verri, W. A. & Chiu, I. M. Nociceptor Sensory Neuron–Immune Interactions in
801 Pain and Inflammation. *Trends Immunol.* **38,** 5–19 (2017).
802 54. Donoviel, M. S. *et al.* Spinster 2, a sphingosine 1-phosphate transporter, plays a Critical Role in
803 inflammatory and Autoimmune Diseases. *FASEB J.* **29,** 5018–5028 (2015).
804 55. Gräler, M. H. & Goetzl, E. J. The immunosuppressant FTY720 down-regulates sphingosine 1-
805 phosphate G-protein-coupled receptors. *FASEB J.* **18,** 551–553 (2004).
806 56. Olivera, A., Allende, M. L. & Proia, R. L. Shaping the landscape: Metabolic regulation of S1P
807 gradients. *Biochim. Biophys. Acta - Mol. Cell Biol. Lipids* **1831,** 193–202 (2013).
808 57. Allende, M. L. *et al.* Sphingosine-1-phosphate lyase deficiency produces a pro-inflammatory
809 response while impairing neutrophil trafficking. *J. Biol. Chem.* **286,** 7348–7358 (2011).
810 58. Kunkel, G. T., Maceyka, M., Milstien, S. & Spiegel, S. Targeting the sphingosine-1-phosphate axis in
811 cancer, inflammation and beyond. *Nat. Rev. Drug Discov.* **12,** 688–702 (2013).
812 59. Roviezzo, F. *et al.* S1P-induced airway smooth muscle hyperresponsiveness and lung inflammation
813 in vivo: Molecular and cellular mechanisms. *Br. J. Pharmacol.* **172,** 1882–1893 (2015).
814 60. Liang, J. *et al.* Sphingosine-1-Phosphate Links Persistent STAT3 Activation, Chronic Intestinal
815 Inflammation, and Development of Colitis-Associated Cancer. *Cancer Cell* **23,** 107–120 (2013).
816 61. Rivera, J., Proia, R. L. & Olivera, A. The alliance of sphingosine-1-phosphate and its receptors in
817 immunity. *Nat. Rev. Immunol.* **8,** 753–763 (2008).
818 62. Myśliwiec, H. *et al.* Increase in circulating sphingosine-1-phosphate and decrease in ceramide levels
819 in psoriatic patients. *Arch. Dermatol. Res.* (2016). doi:10.1007/s00403-016-1709-9
820 63. Checa, A. *et al.* Circulating levels of sphingosine-1-phosphate are elevated in severe, but not mild
821 psoriasis and are unresponsive to anti-TNF-α treatment. *Sci. Rep.* **5,** 12017 (2015).
822 64. Grenald, S. A. *et al.* Targeting the S1P/S1PR1 axis mitigates cancer-induced bone pain and
823 neuroinflammation. *Pain* **158,** 1 (2017).
824 65. Trankner, D., Hahne, N., Sugino, K., Hoon, M. A. & Zuker, C. Population of sensory neurons

825 essential for asthmatic hyperreactivity of inflamed airways. *Proc. Natl. Acad. Sci.* **111,** 11515–11520
826 (2014).
827 66. Wilson, S. R. *et al.* The Ion Channel TRPA1 Is Required for Chronic Itch. *J. Neurosci.* **33,** 9283–
828 9294 (2013).
829 67. Tsunozaki, M. *et al.* A 'toothache tree' alkylamide inhibits Aδ mechanonociceptors to alleviate
830 mechanical pain. *J. Physiol.* **591,** 3325–40 (2013).
831 68. Shimada, S. G. & LaMotte, R. H. Behavioral differentiation between itch and pain in mouse. *Pain*
832 **139,** 681–687 (2008).
833 69. Chaplan, S.R., Bach, F.W., Pogrel, J.W., Chung, J.M., Yaksh, T. Quantitative assessment of tactile
834 allodynia evoked by unilateral ligation of the fifth and sixth lumbar nerves in the rat. *J. Neurosci.* **53,**
835 55–63 (1994).
836 70. Dixon, W. J. The Up-and-Down Method for Small Samples. *J. Am. Stat. Assoc.* **60,** 967–978 (1980).
837 71. Marshall, K. L. *et al.* Touch Receptors Undergo Rapid Remodeling in Healthy Skin. *Cell Rep.* **17,**
838 1719–1727 (2016).
839 72. Wilson, S. R. *et al.* TRPA1 is required for histamine-independent, Mas-related G protein-coupled
840 receptor-mediated itch. *Nat. Neurosci.* **14,** 595–602 (2011).
841 73. Zheng, Q. *et al.* Suppression of KCNQ/M (Kv7) potassium channels in dorsal root ganglion neurons
842 contributes to the development of bone cancer pain in a rat model. *Pain* **154,** 434–448 (2013).
843 74. Wellnitz, S. A., Lesniak, D. R., Gerling, G. J. & Lumpkin, E. A. The Regularity of Sustained Firing
844 Reveals Two Populations of Slowly Adapting Touch Receptors in Mouse Hairy Skin. *J.*
845 *Neurophysiol.* **103,** 3378–3388 (2010).
846 75. Maksimovic, S. *et al.* Epidermal Merkel cells are mechanosensory cells that tune mammalian touch
847 receptors. *Nature* **509,** 617–621 (2014).
848 76. Koltzenburg, M. *et al.* Receptive Properties of Mouse Sensory Neurons Innervating Hairy Skin
849 Receptive Properties of Mouse Sensory Neurons Innervating Hairy Skin. *J. Neurophysiol.* **78,** 1841–
850 1850 (1997).
851 77. Zimmermann, K. *et al.* Phenotyping sensory nerve endings in vitro in the mouse. *Nat. Protoc.* **4,**
852 174–196 (2009).

Figure captions

Figure 1. S1PR3 mediates acute mechanical pain. A. von Frey 50% withdrawal threshold measurements for *S1pr3*$^{+/+}$ (WT, N = 8), $^{+/-}$ (HET, N = 7) and $^{-/-}$ (KO, N = 12) mice. $p < 0.0001$ (one-way ANOVA). Tukey-Kramer post hoc comparisons for KO and HET to WT indicated on graph. **B.** von Frey force-response graph for WT (N = 8) versus KO (N = 12) animals; $p_{genotype} < 0.0001$ (two-way ANOVA). Tukey HSD comparisons between genotypes are indicated for given forces. **C.** % withdrawal to pinprick stimulation of hindpaw for HET versus KO animals; $p < 0.0001$ (unpaired t-test; N = 5-7 mice per group). **D.** Number of attempted removal bouts in tape assay for WT (N =2), HET (N = 2), and KO (N = 5) mice; $p = 0.172$ (one-way ANOVA). **E.** Baseline radiant heat measurements for WT, HET, and KO mice. N = 8 WT, 3 HET, and 5 KO mice. $p = 0.444$ (one-way ANOVA). **F.** von Frey 50% withdrawal threshold measurements for mice pre- and post-injection of 500 µM TY 52156 (N = 10), 10 µM W146 (N = 6), or 1% DMSO-PBS vehicle (N = 17); $p = 0.016$, 0.650 (two-tailed paired t-test comparing vehicle- vs. drug-injected paw). **G.** von Frey force-response graph for mice injected with either 1% DMSO-PBS or 500 µM TY 52156; $p_{treatment} <$ 1e-05 (two-way ANOVA; N = 4 mice per group). Tukey HSD comparisons were made between treatment groups and significant differences at a given force are indicated on graph. Error bars represent mean ± SD.

Figure 1-source data 1. S1PR3 mediates acute mechanical pain. *Related to Figure 1.*

Figure 1-figure supplement 1. Loss of S1PR3 selectively impairs mechanonociception. *Related to Figure 1.* **A.** Time to righting in seconds for N = 6 P7 pups per genotype for WT and KO mice; $p = 0.575$ (two-tailed unpaired t-test). **B.** (Left) Time spent scratching in response to injection of 50 mM chloroquine or PBS vehicle (VEH) in WT and KO mice; $p = 0.36$, 0.98, (unpaired t-tests; N = 3-4 mice per group). (Right) Time spent scratching in response to injection of 27 mM Histamine or 0.1% DMSO-PBS in WT and KO mice; $p = 0.51$, 0.06 (unpaired t-tests; N = 3-4 mice per group). **C.** Normalized paw withdrawal latencies post-injection of SKI II, TY 52156, or 0.1% DMSO-PBS vehicle into the hind paw of wild-type animals; $p = 0.65$ (one-way ANOVA); N = 5 mice per group. Unless otherwise indicated, error bars represent mean ± SD.

881

882 **Figure 2. Endogenous S1P mediates acute mechanical pain. A.** von Frey 50% withdrawal
883 measurements for mice pre- and post-injection of 50 µM SKI II (N = 8) or 10 µM S1P (N = 7); p = 0.003,
884 0.604 (two-tailed paired t-tests). **B.** von Frey force-response graph for animals injected with 10 µM S1P or
885 0.1% MeOH-PBS; $p_{genotype}$ > 0.05 (two-way ANOVA; N = 8 mice per group). No Tukey HSD comparisons
886 at any force between genotypes were significant. **C.** Intradermal cheek injection of 10 µM S1P, 2 µM, 0.2
887 µM, and 20 µL 0.3% methanol PBS (vehicle), with quantification of number of forepaw wipes over the 5
888 minute post-injection interval; p < 0.0001 (one-way ANOVA; N = 3 mice per condition). Dunnett's multiple
889 comparisons p-values are represented on graph for comparisons made between treated and vehicle
890 groups. **D.** Radiant heat normalized paw withdrawal latencies 20-30 minutes post injection of 15 µL 10 µM
891 S1P, 0.2 µM S1P. or 0.3% methanol-PBS vehicle (i.d.) into the hind paw of S1PR3 WT or KO mice; p =
892 0.0129 (one-way ANOVA; N = 3-10 mice per condition). Dunnett's multiple comparisons p-values are
893 represented on graph for comparisons made between treated and vehicle groups. **E.** von Frey 50%
894 withdrawal measurements for mice pre- (baseline) and post-injection of 50 µM SKI II (N = 14) and 0, 10,
895 75, or 200 nM S1P (one-way ANOVA, p = 0.0001; N = 4, 3, 4, 3 animals). Tukey Kramer comparisons are
896 indicated on graph. Error bars represent mean ± SD.

897

898 **Figure 2-source data 1. Endogenous S1P mediates acute mechanical pain.** *Related to Figure 2.*

899

900 **Figure 3. *S1pr3* is expressed in A mechanonociceptors and C thermal nociceptors. A.** (Top)
901 Representative co-ISH of *S1pr3* (green; left) with *Scn1a*, *Npy2r*, *Piezo2*, and *Trpv1* (magenta; center) in
902 sectioned DRG. Right column: overlay with co-localized regions colored white (10x air objective; scale =
903 100 µm). **B.** Bar chart showing the % of total cells expressing the indicated marker (grey) and the % of total
904 cells co-expressing both marker and *S1pr3* (green). See Table S1 for quantification. **C.** Representative IHC
905 images of sectioned DRG from *S1pr3*$^{mCherry/+}$ animals stained with anti-DsRed (green, S1PR3) and anti-
906 Peripherin (left, magenta) or anti-NF200 (right, magenta). Arrows indicate co-stained cells. Images were
907 acquired using a 10x air objective (scale = 100 µm). **D.** Whole-mount skin IHC confocal images with anti-
908 DsRed antibody (S1PR3, green) and anti-NefH antibody (NF200, magenta) in an *S1pr3*$^{mCherry/+}$ animal (20x

909 water objective; scale = 50 µm). Arrows indicate co-positive free nerves (left image). Arrowheads indicate
910 NF200- free nerves (left) or S1PR3- circumferential fibers (right image). **E.** Sectioned skin IHC with anti-
911 DsRed (S1PR3) and anti-NefH (NF200, left, top right) or anti-DsRed (S1PR3) and anti-beta-tubulin III
912 (BTIII, bottom right) antibody (magenta) in *S1pr3*$^{mCherry/+}$ skin (20x air objective; scale = 50 µm). Arrows
913 indicate co-positive free nerve endings (left), S1PR3-negative lanceolate/circumferential hair follicle
914 endings (top right, arrow = circumferential, arrowhead = lanceolate), or S1PR3-negative putative Merkel
915 afferent (bottom right). **F.** (Left) Quantification of sectioned DRG IHC experiments showing % of S1PR3+
916 cells that co-stained with indicated markers (n > 250 cells per marker). (Right) Quantification of sectioned
917 skin IHC experiments showing % of fibers positive for indicated marker that co-stained with S1PR3 (anti-
918 DsRed; n = 10 images per marker from 2 animals).
919
920 **Figure 3-figure supplement 1. S1PR3 KO animals display normal representation of somatosensory**
921 **neuronal subtypes.** *Related to Figure 3.* **A.** ISH of sectioned adult DRG from WT and S1PR3 KO animals
922 showing specificity of *S1pr3* probes (20x air objective, scale = 50 µm). **B.** (Image) Representative ISH
923 *Trpv1* (top) and *Trpa1* (bottom) from sectioned DRG of wild-type (left) and S1PR3 KO animals (right; 20x
924 air objective; scale = 50 µm). **C.** % of total cells expressing *Trpv1* and *Trpa1* in sectioned DRG of wild-type
925 and S1PR3 KO animals. **D.** (Left) Average diameter ± SEM of all cells in sectioned DRG from WT and
926 S1PR3 KO animals (p = 0.36, t-test; n = 437 and 679 cells from two animals each, respectively). (Right)
927 Average diameter ± SD of *Trpv1+* cells in WT and S1PR3 KO DRG (p = 0.63, t-test; n = 127 and 85 cells
928 respectively). **E.** Representative staining with anti-S1PR3 antibody (1:2000) in sectioned adult DRG from
929 WT and S1PR3 KO animals (10x air objective, scale = 100 µm). **F.** Representative IHC images of
930 sectioned DRG from S1PR3 KO animals stained with anti-DsRed (green) and anti-Peripherin (left,
931 magenta) or anti-NF200 (right, magenta). Images were acquired using a 10x air objective (scale = 100 µm).
932 **G.** (Left) Quantification of total percentage of cells stained with indicated markers in sectioned DRG from
933 *S1pr3*$^{mCherry/+}$ and S1PR3 KO animals (n > 250 cells per condition). (Right) Average diameter of anti-
934 NF200+ cells in *S1pr3*$^{mCherry/+}$ and S1PR3 KO DRG (p = 0.15, t-test; n = 256 and 194 cells, respectively). **H.**
935 Percent responders to S1P and capsaicin in ratiometric calcium imaging of wild-type and *S1pr3* $^{-/-}$ cultured
936 DRG and TG neurons; p < 0.0001 (one-way ANOVA; N = 2 DRG and 2 TG preparations of 8 wells each).

937 Sidak's multiple comparisons *p*-values are represented on graph for comparisons made between
938 genotypes. Error bars represent mean ± SEM. **I.** (Left) No primary control showing robust staining of hair
939 follicles in whole mount skin in contrast to specific neuronal staining shown in **Figure 3D**. (Right) No
940 primary control showing staining around hair follicles and in epidermis in sectioned skin. Scale = 50 µm
941 (20x water objective).
942
943 **Supplementary file 1. Co-ISH quantification for sectioned DRG from adult wild-type mice.** *Related to*
944 *Figure 3.*
945
946 **Figure 4. S1P activates thermal nociceptors but not mechanonociceptors. A.** (Left) Representative
947 image of mCherry signal in live, cultured adult DRG neurons from one *S1pr3*$^{mCherry/+}$ animal. (Right)
948 Quantification of % of total cells expressing *S1pr3* from DRG ISH and mCherry from dissociated DRG
949 cultures (N = 2 animals each experiment). **B.** Representative traces depicting F340/F380 signal from
950 Fura2-AM calcium imaging showing two neurons, one which responded to 1 µM S1P, 1 µM Capsaicin, and
951 high K+ Ringer's (red) and one which only responded to high K+ (black). **C.** (Left) Fura-2 AM calcium
952 imaging before (left) and after (center) addition of 1 µM S1P in *S1pr3* $^{mCherry/+}$ cultured mouse DRG neurons.
953 Bar indicates fluorescence ratio. Right-hand image indicates mCherry fluorescence. (Right) % of mCherry
954 neurons that are responsive to 1 µM S1P in ratiometric calcium imaging (n > 1000 cells from 16 imaging
955 wells from three animals). **D.** Dose-response curve of mean neuronal calcium responders to varying
956 concentrations of S1P. Concentrations used: 1, 10, 50, 100, 200, 1000, and 10,000 nanomolar. Error bars
957 represent mean ± SD (N = 2 animals). Black dotted line indicates sigmoidal fit for all S1P responders from
958 which EC_{50} was derived. All S1P responders were also capsaicin-responsive. **E.** Current-clamp trace of a
959 single wild-type neuron firing action potentials in response to bath addition of 1 µM S1P and 1 µM
960 capsaicin, with Ringer's wash in-between. n = 4 of 10 neurons responded to S1P and N = 1 of 1 S1P-
961 responsive also responded to capsaicin. Bar = 2 seconds. **F.** (Left) Fura-2 AM calcium imaging after
962 addition of 500 nM Hm1a in *S1pr3*$^{mCherry/+}$ P0 TG neurons, which were instead of adult DRG neurons
963 because they respond to Hm1a without prior PGE_2 sensitization. Right-hand image indicates mCherry
964 fluorescence. (Right) % of Hm1a-responsive P0 TG neurons that are mCherry+ (N = 1 animal, 1230 total

neurons).

Figure 5. S1PR3 modulates KCNQ2/3 channels to regulate AM excitability. All experiments were performed in *S1pr3*$^{mCherry/+}$ or $^{-/-}$ DRG neurons. **A.** (Left) Example traces of a single mCherry+ neuron in whole cell current clamp before and after S1P application. (Right) % change in rheobase after S1P application for *S1pr3*$^{mCherry/+}$ (left) and KO (right) neurons ($p_{WT,KO}$ = 0.012, 0.287; two-tailed paired t-tests; N = 7, 12 cells). **B.** % Δ in input resistance after S1P or vehicle application (p = 0.017; two-tailed paired t-test; N = 4 cells per group). **C.** The S1P-sensitive current is carried by potassium. The current-voltage relationship was determined by subtraction of the post-S1P current from the pre-S1P current and reverses at -60.125 mV; N = 6 cells. Data were fitted with a Boltzmann equation. Pre- and post-S1P currents were measured at the indicated voltage (-100 mV to +80 mV, 20 mV increments) following a +100 mV step (100 ms). Current was quantified using the peak absolute value of the slowly-deactivating current 0-10 ms after stepping to indicated voltage. Unless indicated otherwise, all error bars represent mean ± SEOM. **D.** (Graphic, top) Averaged current traces of a single mCherry+ neuron in whole cell voltage clamp recording comparing tail currents ($\Delta_{I\ tail}$) pre- and post-S1P using indicated voltage step protocol. (graphic, bottom) Averaged current traces of a single mCherry+ neuron in whole cell voltage clamp recording with XE991 treatment. Holding phase (-40 mV, 150 ms) was truncated in traces. (Left graph) % Δ in outward tail current (average +/- SD after indicated treatments (1 μM S1P, 3 μM XE 991, or both) for *S1pr3*$^{mCherry/+}$ medium-diameter neurons; (p = 0.58; one-way ANOVA; n = 6, 8, 14 cells) using protocol depicted at right. (Right graph) % Δ in inward tail current after indicated treatments (LINO = 100 μM linopirdine) for *S1pr3*$^{mCherry/+}$ medium-diameter neurons; (p = 0.47; two-tailed paired t-test; N = 12 cells).

Figure 5-source data 1. S1PR3 modulates KCNQ2/3 channels to regulate AM excitability. *Related to Figure 5.*

Figure 5-figure supplement 1. S1P selectively modulates potassium tail currents to increase DRG neuron excitability. *Related to Figure 5.* **A.** (Left) Example trace of a single mCherry+ neuron in S1P before and after current injection. (Right) Resting membrane potential (RMP) in millivolts before and after

addition of S1P (p = 0.23; two-tailed paired t-test; n = 6 cells). **B.** Rheobase pre- and post-S1P application in DRG neurons; p_{WT} = 0.011; p_{KO} = 0.28 (two-tailed paired t-test). Same data are represented in **Figure 5A**. **C.** Sodium I-V relationship for a representative *S1pr3*$^{mCherry/+}$ medium-diameter neuron pre- and 5 minutes post- 1 µM S1P using voltage step from -100 to +80 mV (150 ms steps, -80 mV holding). **D.** Steady-state I-V relationship for same neuron. **E.** (Left) % Δ in peak sodium current (Na^+) after S1P or 1% DMSO vehicle application for medium-diameter mCherry+ neurons; p = 0.39 (two-tailed paired t-test; n = 7 cells per group). (Right) % Δ in peak steady-state current (S.S. K^+) after S1P or 1% DMSO vehicle application for medium-diameter mCherry+ neurons; p = 0.948 (two-tailed paired t-test; n = 7 cells per group). **F.** % Δ in inward tail current ($\Delta_{I\ tail}$) after S1P or 1% DMSO vehicle application for *S1pr3*$^{mCherry/+}$ and KO medium-diameter neurons using a pre-pulse stimulation of +80 mV followed by a step to -80 mV, where ($\Delta_{I\ tail}$) was calculated by subtracting the steady-state current from the absolute peak of the slowly-deactivating current at -80 mV (p = 0.014; one-way ANOVA; N = 10, 13, 10 cells). Tukey Kramer post hoc p-values indicated on graph. **G.** Dose-response relationship between % Δ in tail current and S1P concentration for 1 nM, 50 nM, 100 nM, and 1 µM S1P (n = 7 cells). EC_{50} (48.8 nM), marked by thin dotted lines, was estimated from sigmoidal fit (thick dotted line).

Figure 6. S1PR3 is required for nociceptive responses of high-threshold AM nociceptors.

A. (Left) Representative traces of AM fiber activity over time in *ex vivo* skin-saphenous nerve recording in response to stimulation (128 mN, top) from HET (middle) and KO (bottom) mice. (Right) Mean firing rate of AM fibers in response to force controlled stimulation (4, 8, 16, 32, 64, 128, 256 mN). **p=0.001, ***p=0.0002 (two-way ANOVA, Sidak's post-hoc); lines, linear regression (HET: slope=50 Hz/N, R^2=0.99; KO: slope=35 Hz/N, R^2=0.95). **B.** von Frey threshold of AM fibers in S1PR3 HET and KO specimens. ***p < 0.0001 (Mann-Whitney test); lines, median; boxes, 25-75 percentile; whiskers, min-max. **C.** Cumulative response plot of AM fibers to force controlled stimulation (solid lines); four-parameter logistic fit from which half-maximal force was estimated for each genotype (dotted lines). **D.** Conduction velocity (CV) of AM fibers in S1PR3 HET and KO mice. p = 0.65 (two-tailed t-test); n = 40, 36 fibers; errors, mean ± SEM. **E.** Representative traces and binned instantaneous firing frequencies (IFF; 200-ms bins) of Non-Adapting and Adapting AMs in response to force controlled stimulation (256 mN, top) for S1PR3 HET and KO mice;

blue regions, dynamic phase of stimulation (200-ms). **F**. Proportion of fibers classified by pattern of mechanically evoked responses to 256-mN stimuli: Non-Responder (HET, 2/40 fibers; KO 5/36), Non-Adapting AM (HET, 18/40; KO, 29/36), Adapting AM (HET, 20/40; KO, 2/36). Non-Responders fired action potentials to large magnitude von Frey monofilaments (<0.5 mm tip diameter), but not controlled mechanical stimulation (256 mN, 2-mm tip diameter). ***p<0.00001 (Chi-square test).

Figure 6-source data 1. S1PR3 is required for nociceptive responses of high-threshold AM nociceptors. *Related to Figure 6.* Table provides properties of all S1PR3 HET and KO AM fibers that were recorded.

Figure 6-figure supplement 1. S1PR3 HET AM nociceptors display normal nociceptive responses. *Related to Figure 6*. **A.** Mean firing rate of AM fibers in response to force controlled stimulation (4, 8, 16, 32, 64, 128, 256 mN) from **Figure 6A**, with additional data from one wild-type animal (n_{WT} = 4 fibers) (WT: slope, 57 Hz/N, R^2, 0.98; p = 0.90, two-way ANOVA comparing HET and WT). **B.** (Left) Conduction velocities from teased fibers from 6 S1PR3 KO animals (purple, Aβ, centroid=13.1 m/s; yellow, Aδ, centroid=5.7 m/s; orange, C, centroid=0.4 m/s; R^2 =0.69, N = 65 fibers). (Right) Conduction velocities from teased fibers from 1 S1PR3 HET and 6 C57BL/6 WT animals (purple, Aβ, centroid=14.5 m/s; yellow, Aδ, centroid=6.8 m/s; orange, C, centroid=0.3 m/s; R^2 =0.82, N = 76 fibers). Three-term Gaussian model. X-axis plotted on a log 1.2 scale. **C.** Mean firing rates during dynamic (ramp) and static (hold) stimulation for S1PR3 HET and S1PR3 KO recordings (left, Adapting AMs; right, Non-Adapting AMs; see **Figure 6E-F** for experimental details). No significant differences were found between genotypes (p = 0.227, 0.490 (two-way ANOVA); bars, means). As shown in **Figure 6F**, the proportion of Adapting AMs was significantly lower in S1PR3 KO recordings compared with littermate controls.

Figure 7. S1PR3 is dispensable for development of chronic mechanical hypersensitivity. A. Thermal latency before and after CFA treatment (indicated by dotted line); $p_{genotype}$ = 0.0053 (two-way ANOVA; N = 5 mice per genotype). Sidak's multiple comparison between genotypes for specific time points indicated on graph. Error bars represent mean ± SD. **B.** (Left) Normalized 50% withdrawal threshold before and after

CFA treatment (indicated by dotted line); *p*(genotype) < 0.001 (two-way ANOVA). (Right) 50% withdrawal thresholds for same experiment (*p*(genotype) = 0.1634; two-way ANOVA). **C.** (Left) Thermal latency assessed before ("Baseline") and 24 hours post CFA injection with either vehicle (CFA + VEH) or TY 52156 (CFA + TY) acutely administered; $p < 0.0001$ (one-way ANOVA N = 5 mice per treatment). (Right) Thermal latency assessed before and after CFA injection with either vehicle (VEH) or SKI II acutely administered on Day 1; $p < 0.0001$ (one-way ANOVA; N = 5-7 mice per treatment). Dunnett's test comparisons to baseline are indicated on graph. Error bars represent mean ± SD. **D.** (Left) 50% withdrawal threshold assessed before and 24 hours post CFA injection with either vehicle (CFA + VEH) or TY 52156 (CFA + TY) acutely administered on Day 1; $p < 0.0001$ (one-way ANOVA; N = 5 mice per treatment). Dunnett's test comparisons to baseline are indicated on graph. (Right) 50% withdrawal threshold assessed before and 24 hours post CFA injection with either vehicle (CFA + VEH) or SKI II (CFA + SKI II) acutely administered; *p*-values indicated on graph (two-tailed unpaired t-test; N = 5 mice per group.

Figure 7-source data 1. S1PR3 is dispensable for development of chronic mechanical hypersensitivity. *Related to Figure 7.*

Figure 7-figure supplement 1. S1PR3 KO animals display normal CFA-evoked immune cell recruitment. *Related to Figure 7.* **A.** Recruitment of neutrophils (Neut.) or inflammatory monocytes (IMs) to hindpaw skin 24 hours post-CFA administration in S1PR3 HET and KO mice, as a dot plot of CD11b+ cells plotting Ly6G fluorescence intensity vs. Ly6C intensity (AFU). Boxes are for illustrative purposes. **B.** Recruitment of immune cells, including neutrophils (Neut.) and inflammatory monocytes (IMs) to hindpaw skin 24 hours post-CFA administration in HET and KO mice, displayed as total number of cells; N = 8 mice per genotype. Sidak's multiple comparisons were made between HET and KO for each cell type.

Figure 8. Proposed model illustrating a key role for S1PR3 in regulating mechanical pain in AM nociceptors. (Top) S1P promotes activation of S1PR3, which leads to inhibition of KCNQ2/3 currents and promotes normal mechanical pain sensitivity. (Bottom) Diminished S1P or S1PR3 antagonism alleviates inhibition of KCNQ2/3, leading to mechanical pain hyposensitivity.

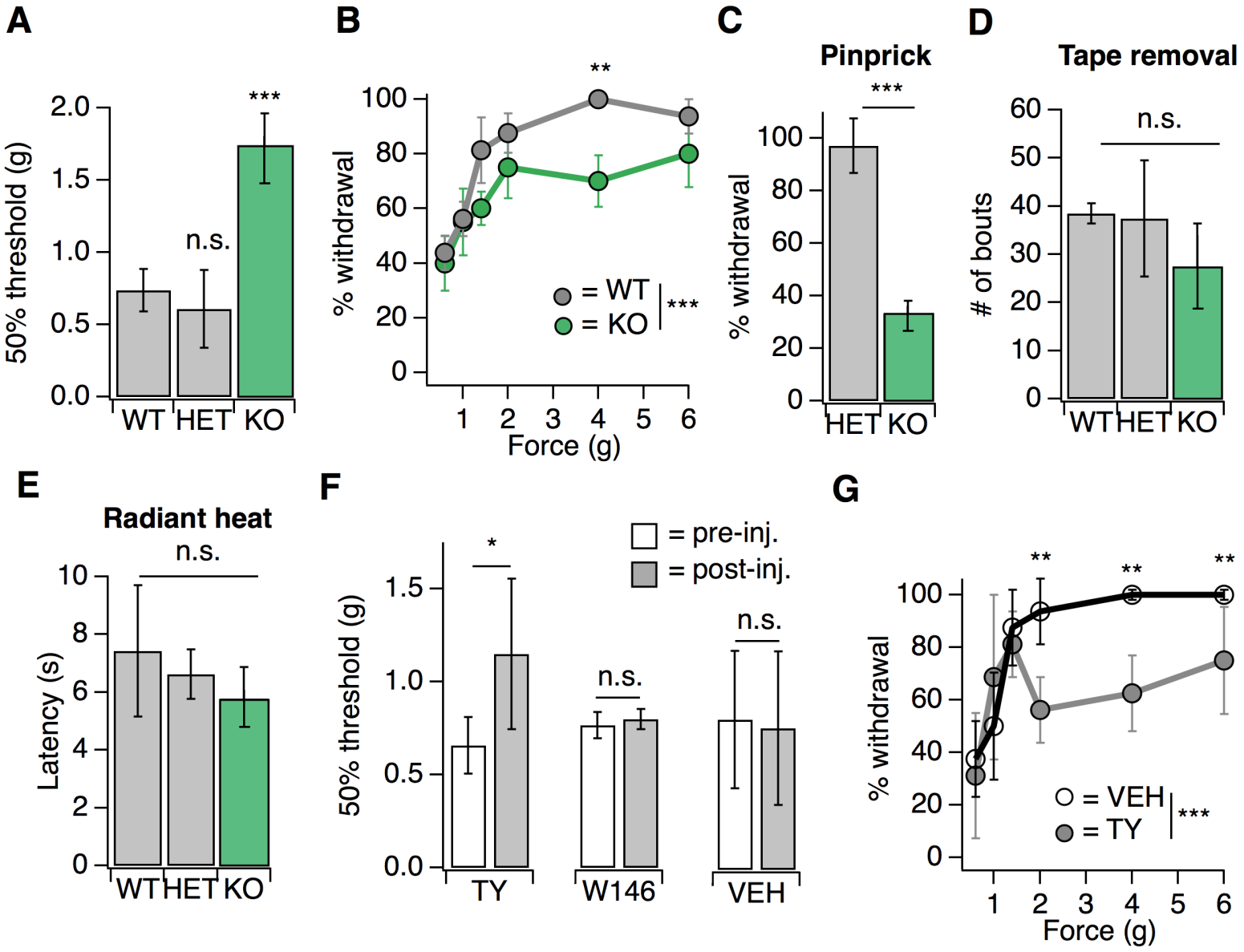
A
50% threshold (g)
2.0
1.5
1.0
0.5
0.0
***
n.s.
WT
HET
KO
B
% withdrawal
100
80
60
40
20
0
**
= WT
= KO
***
1
2
3
4
5
6
Force (g)
C
Pinprick
***
% withdrawal
100
80
60
40
20
0
HET
KO
D
Tape removal
# of bouts
60
50
40
30
20
10
0
n.s.
WT
HET
KO
E
Radiant heat
n.s.
Latency (s)
10
8
6
4
2
0
WT
HET
KO
F
= pre-inj.
= post-inj.
50% threshold (g)
1.5
1.0
0.5
0.0
*
n.s.
n.s.
TY
W146
VEH
G
% withdrawal
100
80
60
40
20
0
**
**
**
= VEH
= TY
***
1
2
3
4
5
6
Force (g)

Figure 1

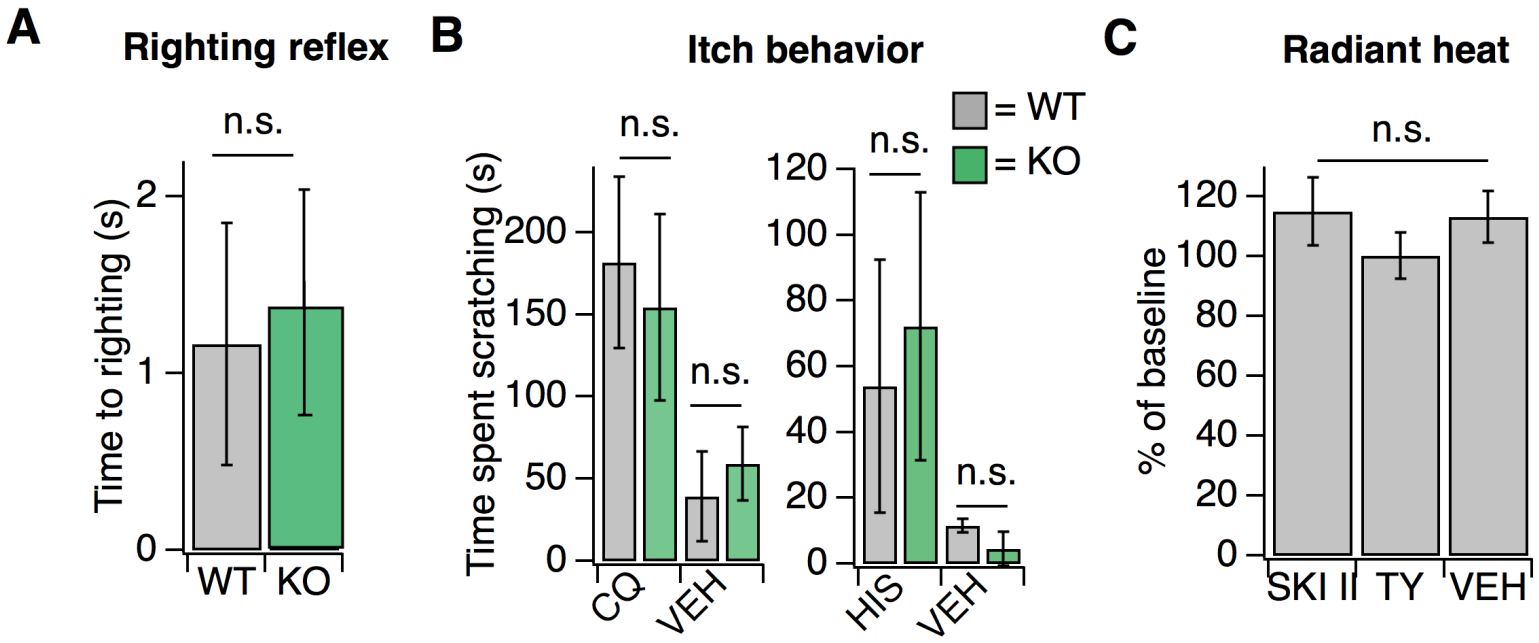

Figure 1-figure supplement 1

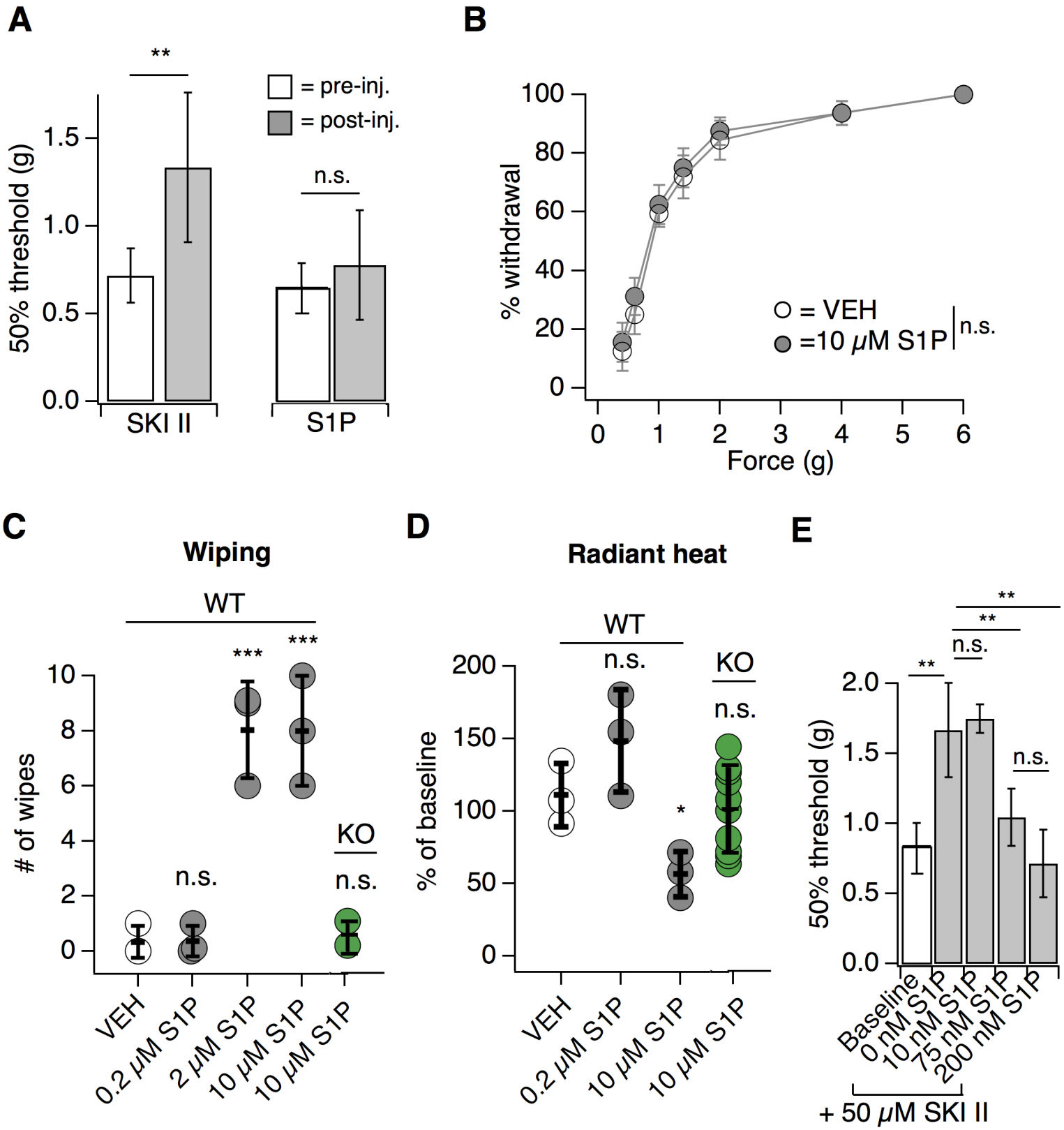
A
**
= pre-inj.
= post-inj.
n.s.
50% threshold (g)
1.5
1.0
0.5
0.0
SKI II
S1P
B
100
80
60
40
20
0
% withdrawal
○ = VEH
● =10 μM S1P
n.s.
0
1
2
3
4
5
6
Force (g)
C
Wiping
WT
***
***
n.s.
KO
n.s.
10
8
6
4
2
0
# of wipes
VEH
0.2 μM S1P
2 μM S1P
10 μM S1P
10 μM S1P
D
Radiant heat
WT
n.s.
KO
n.s.
200
150
100
50
0
% of baseline
*
VEH
0.2 μM S1P
10 μM S1P
10 μM S1P
E
**
**
n.s.
**
n.s.
2.0
1.5
1.0
0.5
0.0
50% threshold (g)
Baseline
0 nM S1P
10 nM S1P
75 nM S1P
200 nM S1P
+ 50 μM SKI II

Figure 2

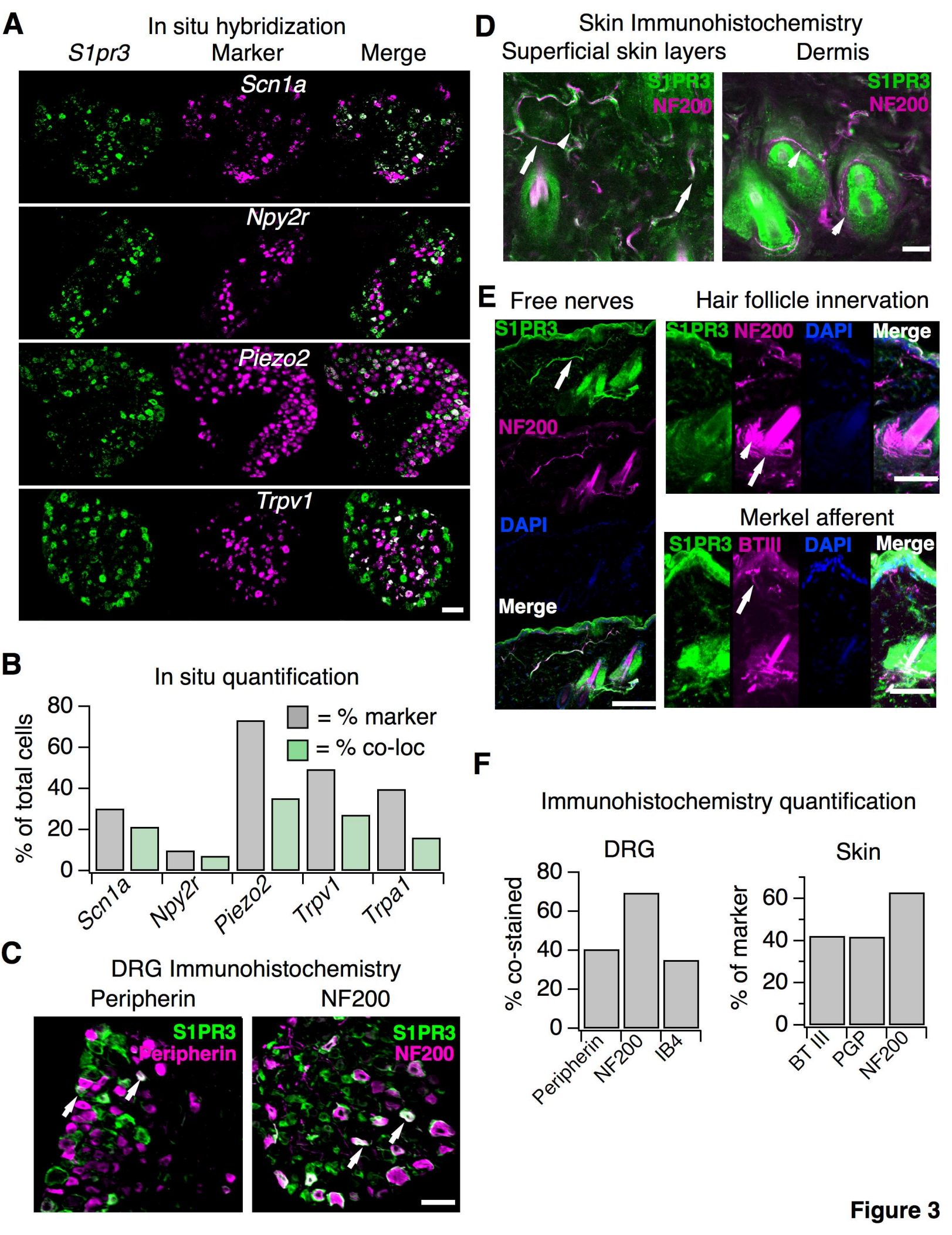
A
In situ hybridization
S1pr3
Marker
Merge
Scn1a
Npy2r
Piezo2
Trpv1
B
In situ quantification
% of total cells
80
60
40
20
0
= % marker
= % co-loc
Scn1a
Npy2r
Piezo2
Trpv1
Trpa1
C
DRG Immunohistochemistry
Peripherin
NF200
S1PR3
Peripherin
S1PR3
NF200
D
Skin Immunohistochemistry
Superficial skin layers
Dermis
S1PR3
NF200
S1PR3
NF200
E
Free nerves
Hair follicle innervation
S1PR3
NF200
DAPI
Merge
S1PR3
NF200
DAPI
Merge
Merkel afferent
S1PR3
BTIII
DAPI
Merge
F
Immunohistochemistry quantification
DRG
% co-stained
80
60
40
20
0
Peripherin
NF200
IB4
Skin
% of marker
60
40
20
0
BT III
PGP
NF200

Figure 3

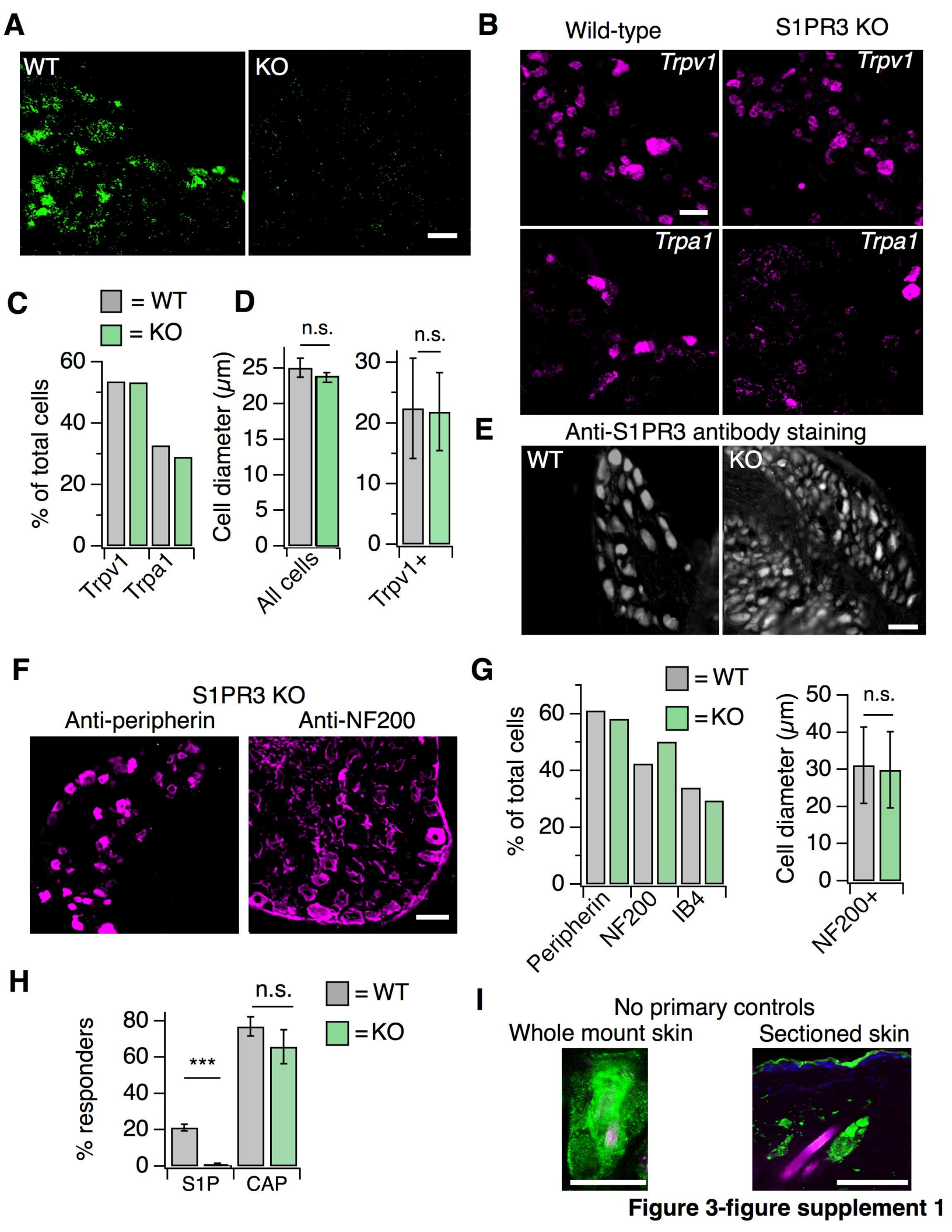

Figure 3-figure supplement 1

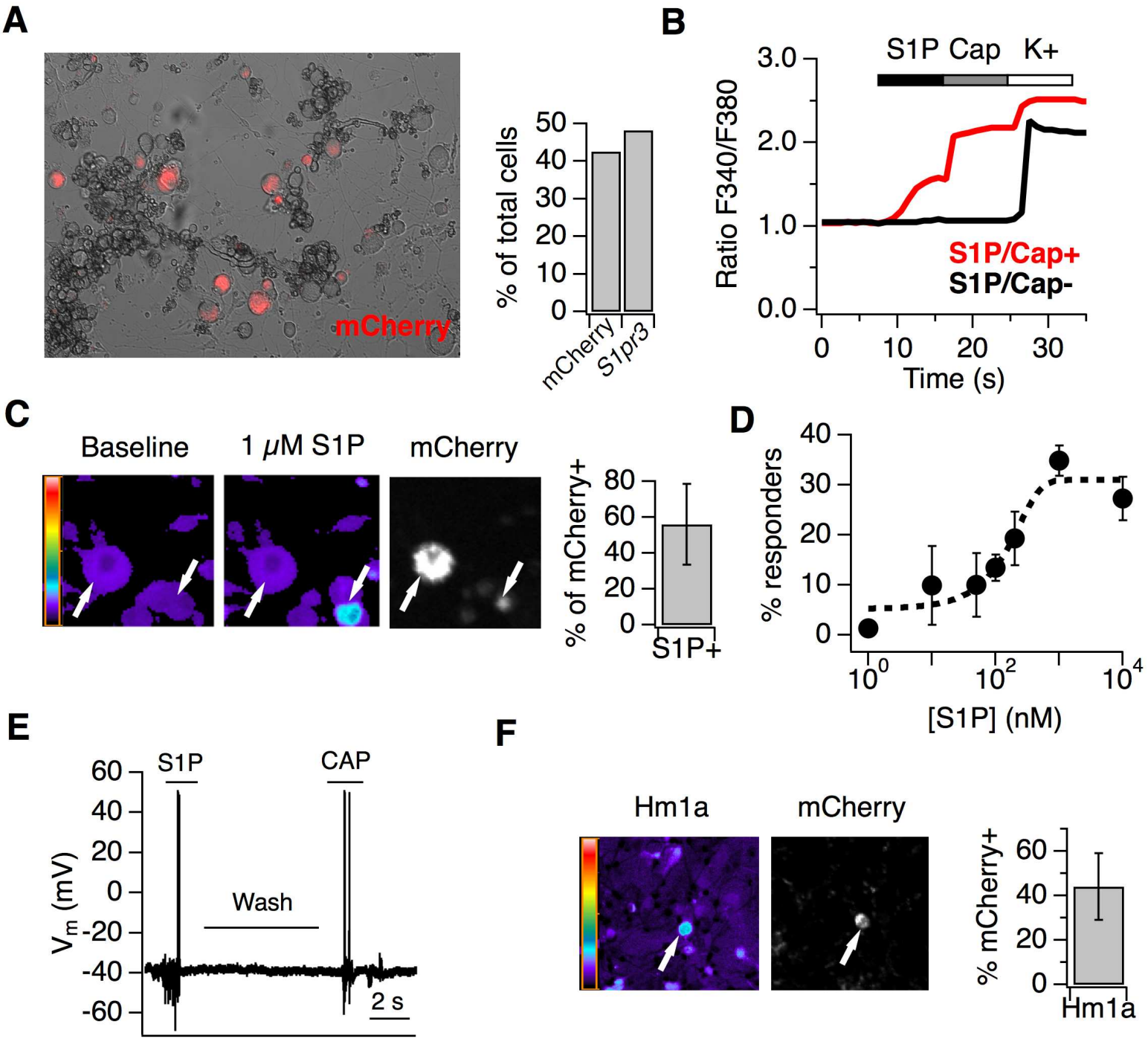
A
mCherry
% of total cells
50
40
30
20
10
0
mCherry
S1pr3
B
S1P Cap K+
3.0
2.0
1.0
0.0
Ratio F340/F380
S1P/Cap+
S1P/Cap-
0
10
20
30
Time (s)
C
Baseline
1 μM S1P
mCherry
% of mCherry+
80
60
40
20
0
S1P+
D
% responders
40
30
20
10
0
10^0
10^2
10^4
[S1P] (nM)
E
S1P
CAP
60
40
20
0
-20
-40
-60
Vm (mV)
Wash
2 s
F
Hm1a
mCherry
% mCherry+
60
40
20
0
Hm1a

Figure 4

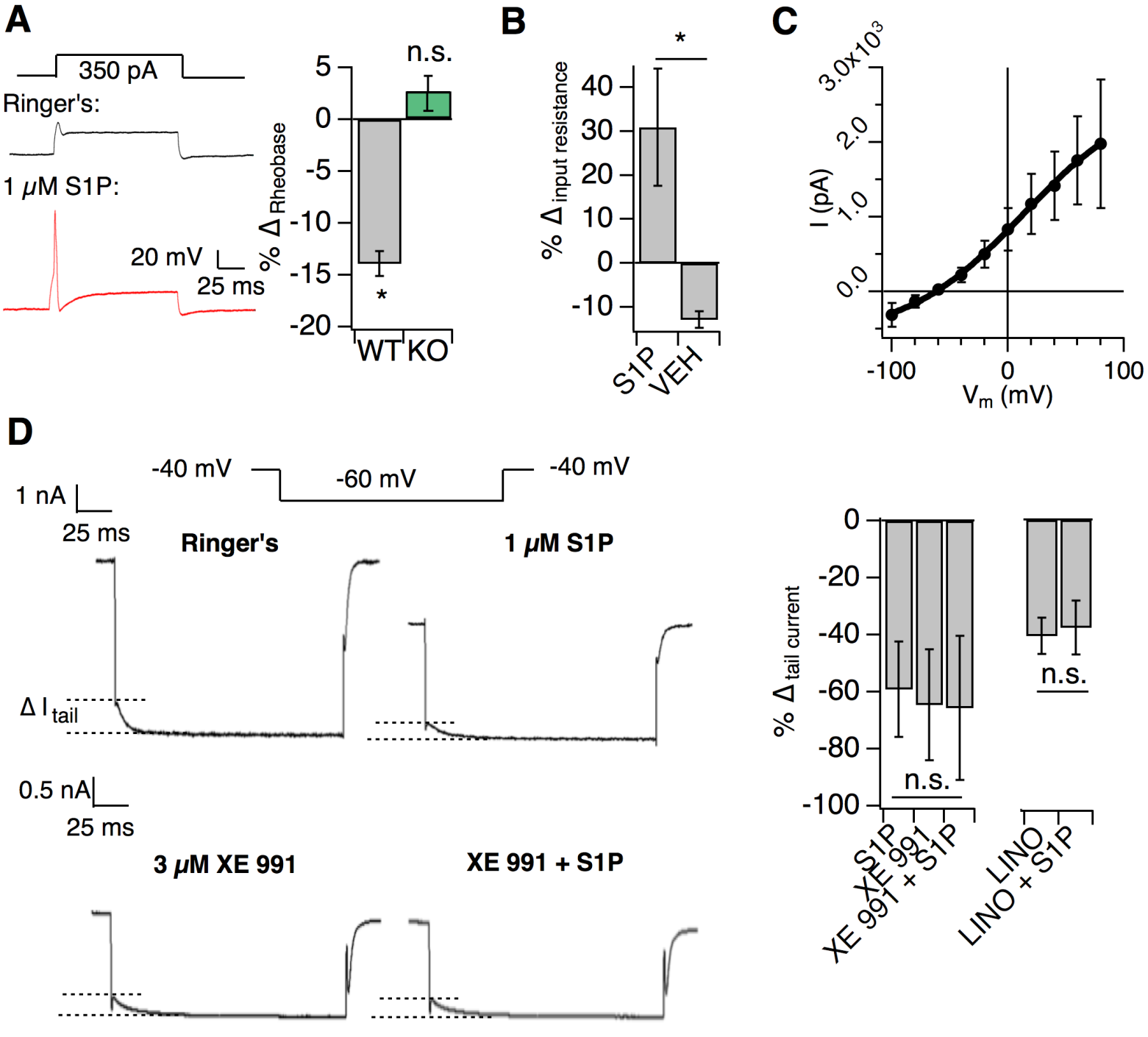
A
350 pA
Ringer's:
1 μM S1P:
20 mV
25 ms
% Δ Rheobase
n.s.
WT
KO
B
% Δ input resistance
S1P
VEH
C
I (pA)
3.0x10³
2.0
1.0
0.0
-100
0
100
Vm (mV)
D
-40 mV
-60 mV
-40 mV
1 nA
25 ms
Ringer's
1 μM S1P
Δ I tail
0.5 nA
25 ms
3 μM XE 991
XE 991 + S1P
% Δ tail current
n.s.
n.s.
S1P
XE 991 + S1P
LINO
LINO + S1P

Figure 5

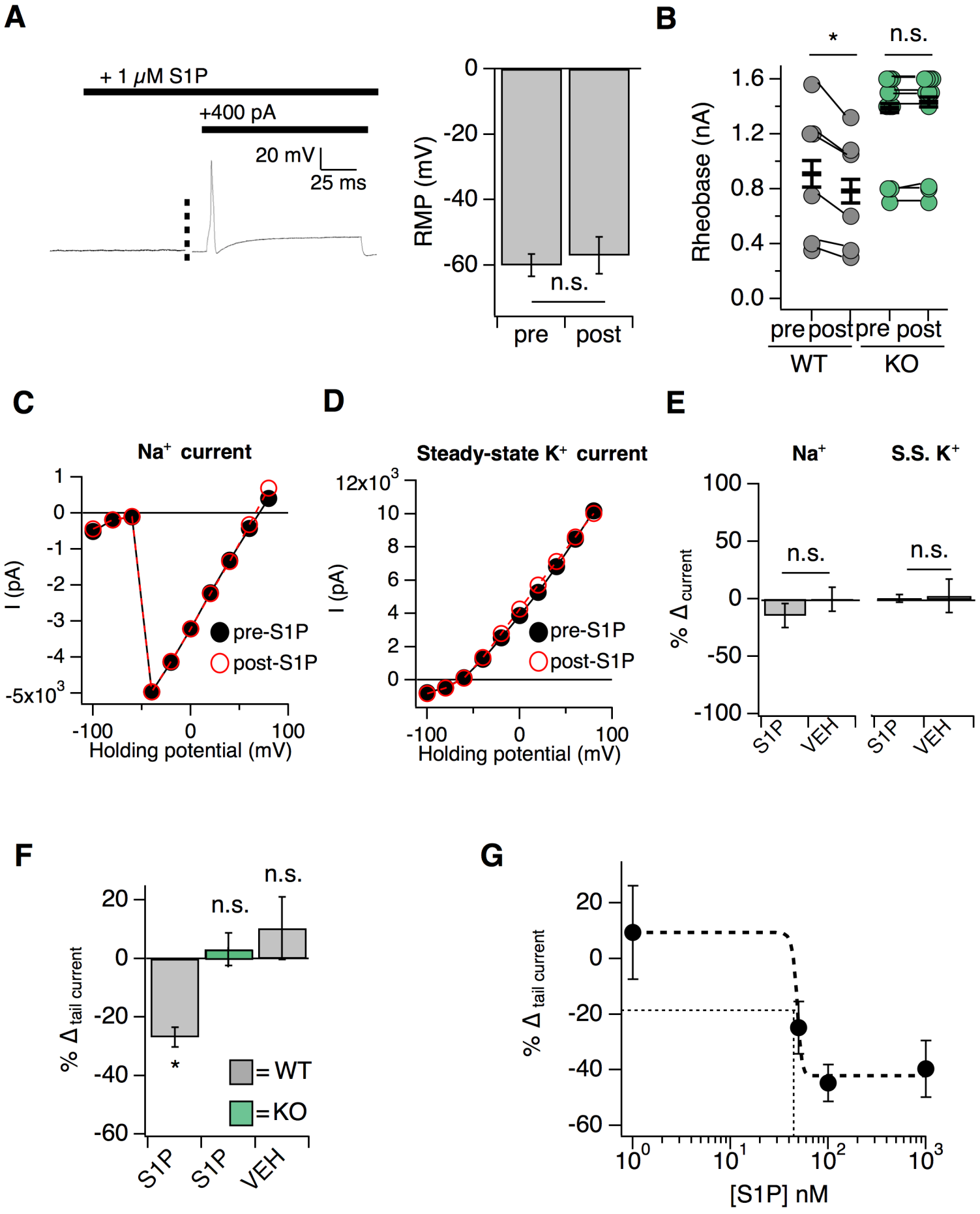

Figure 5-figure supplement 1

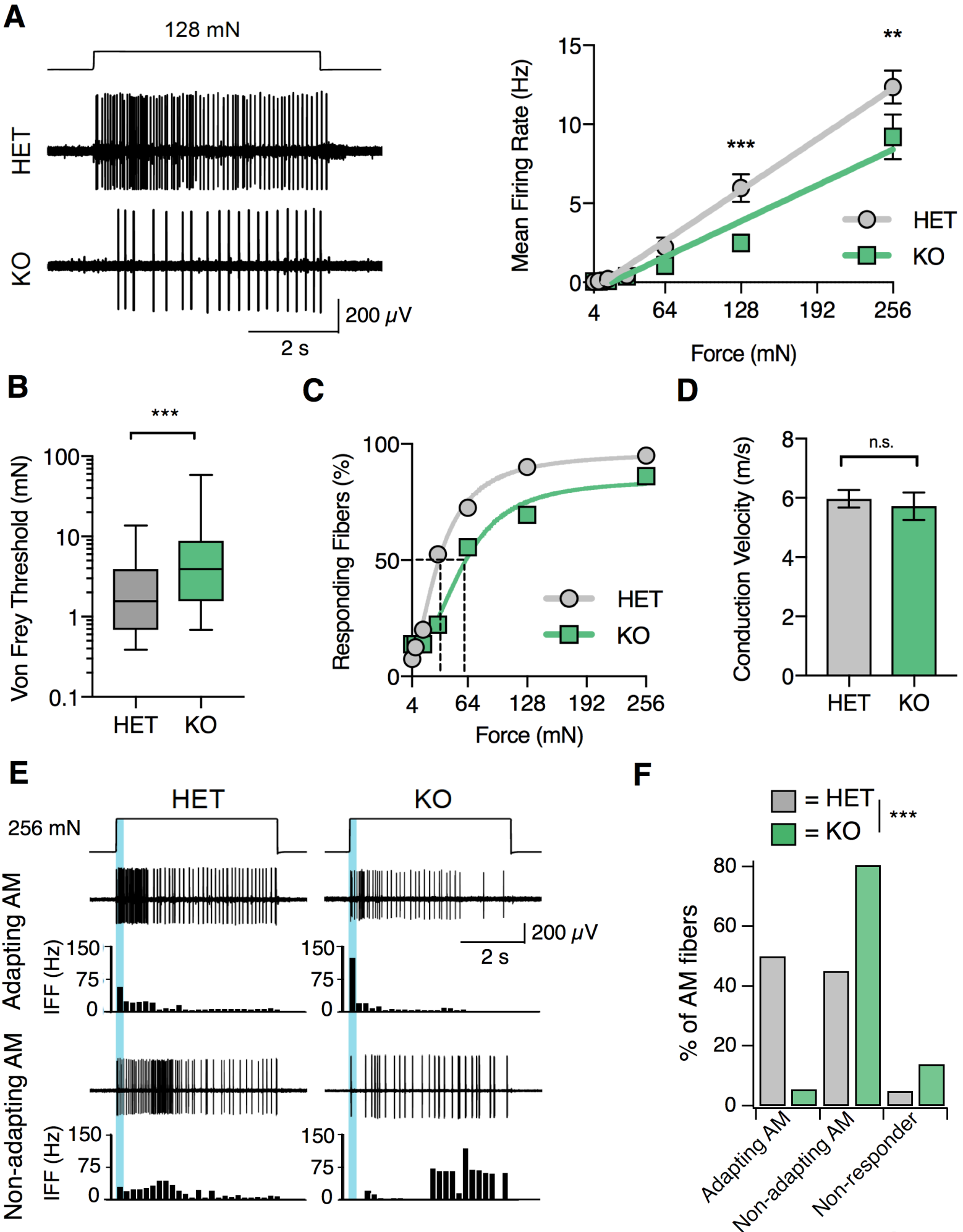
A
128 mN
HET
KO
200 μV
2 s
Mean Firing Rate (Hz)
15
10
5
0
**
***
HET
KO
4
64
128
192
256
Force (mN)
B
***
Von Frey Threshold (mN)
100
10
1
0.1
HET
KO
C
Responding Fibers (%)
100
50
0
HET
KO
4
64
128
192
256
Force (mN)
D
n.s.
Conduction Velocity (m/s)
8
6
4
2
0
HET
KO
E
HET
KO
256 mN
200 μV
2 s
Adapting AM
IFF (Hz)
150
75
0
Non-adapting AM
IFF (Hz)
150
75
0
F
= HET
= KO
***
% of AM fibers
80
60
40
20
0
Adapting AM
Non-adapting AM
Non-responder

Figure 6

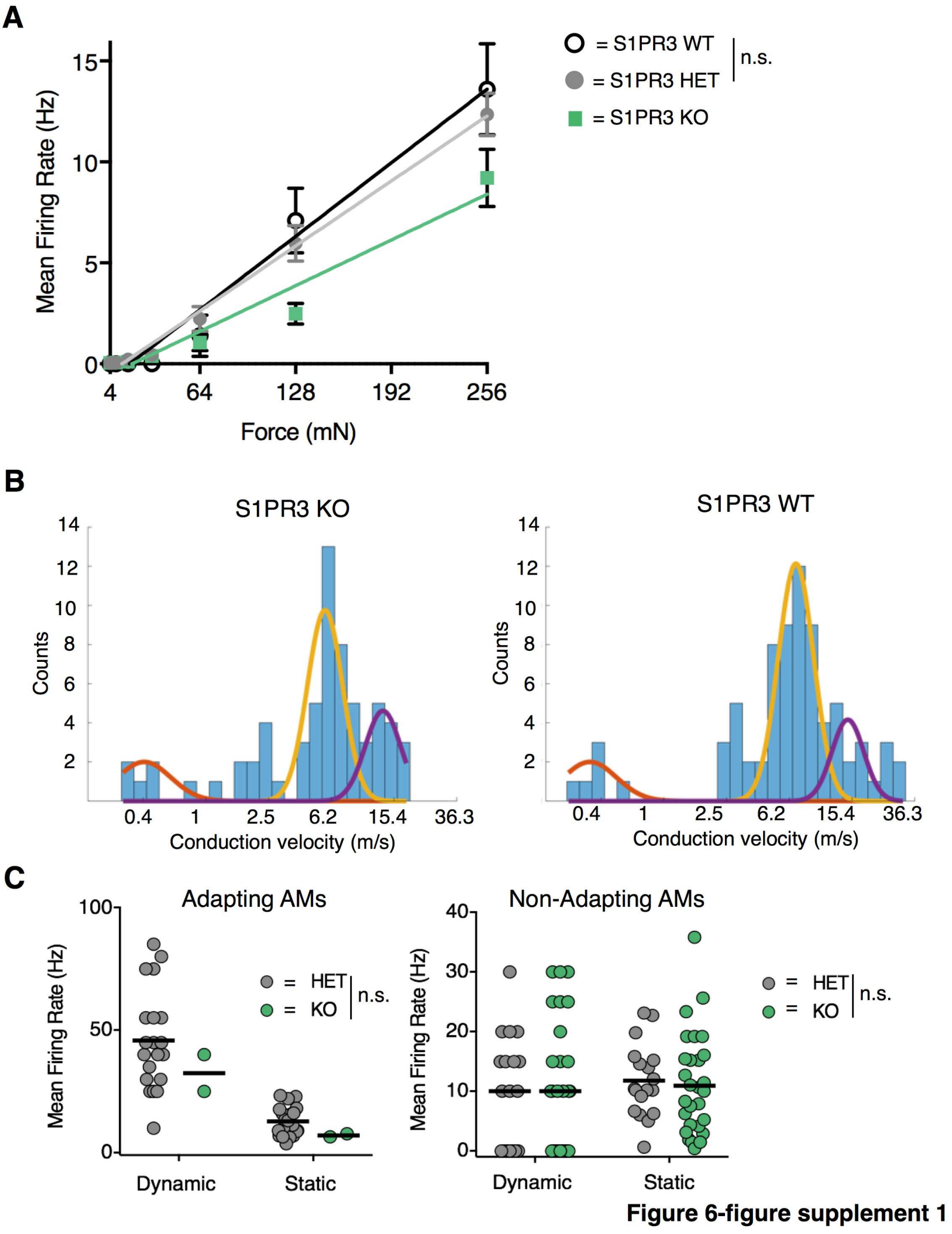

Figure 6-figure supplement 1

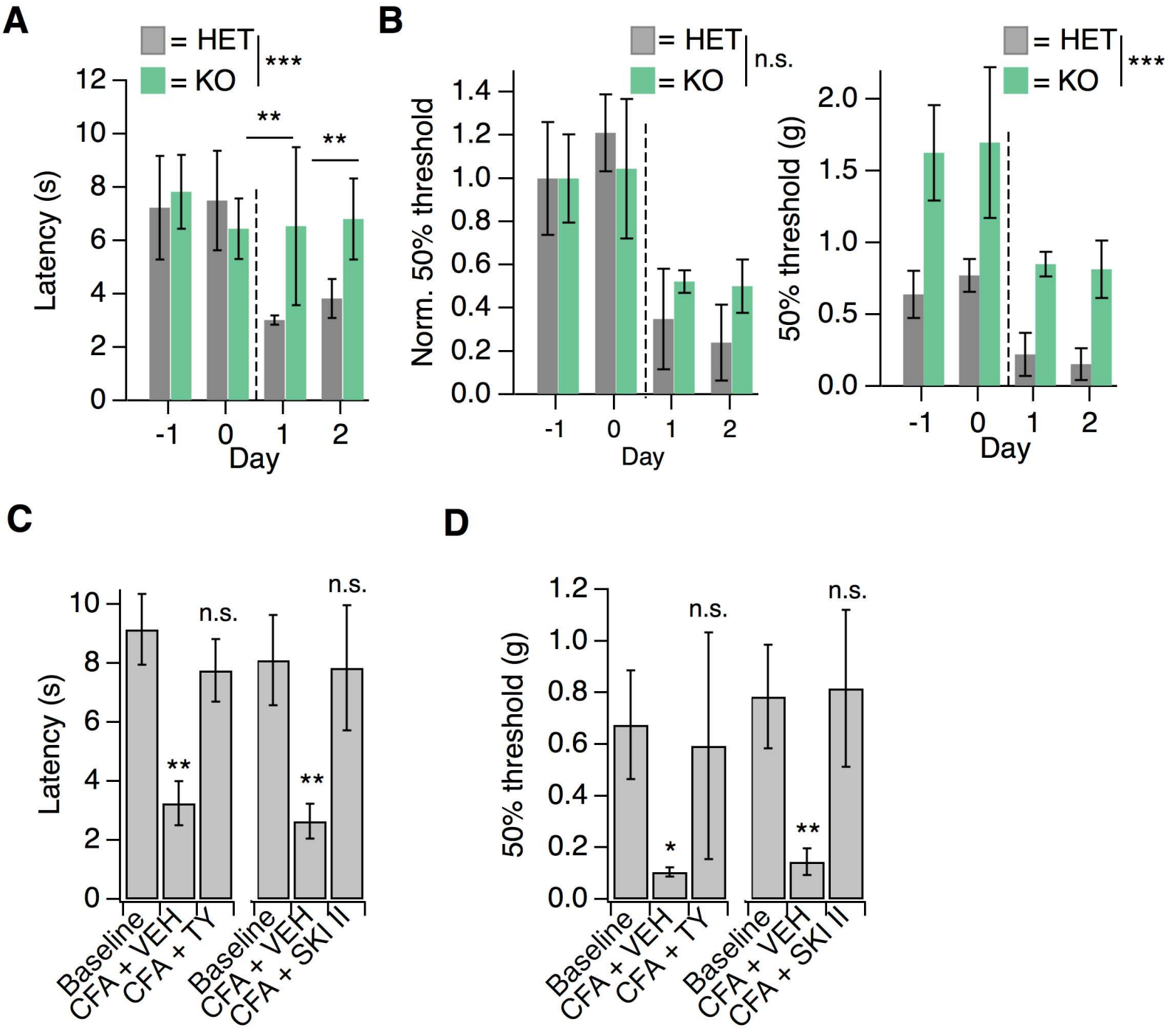
A
= HET
= KO
***
Latency (s)
12
10
8
6
4
2
0
**
**
-1
0
1
2
Day
B
= HET
= KO
n.s.
Norm. 50% threshold
1.4
1.2
1.0
0.8
0.6
0.4
0.2
0.0
-1
0
1
2
Day
= HET
= KO
***
50% threshold (g)
2.0
1.5
1.0
0.5
0.0
-1
0
1
2
Day
C
Latency (s)
10
8
6
4
2
0
n.s.
n.s.
**
**
Baseline
CFA + VEH
CFA + TY
Baseline
CFA + VEH
CFA + SKI II
D
50% threshold (g)
1.2
1.0
0.8
0.6
0.4
0.2
0.0
n.s.
n.s.
*
**
Baseline
CFA + VEH
CFA + TY
Baseline
CFA + VEH
CFA + SKI II

Figure 7

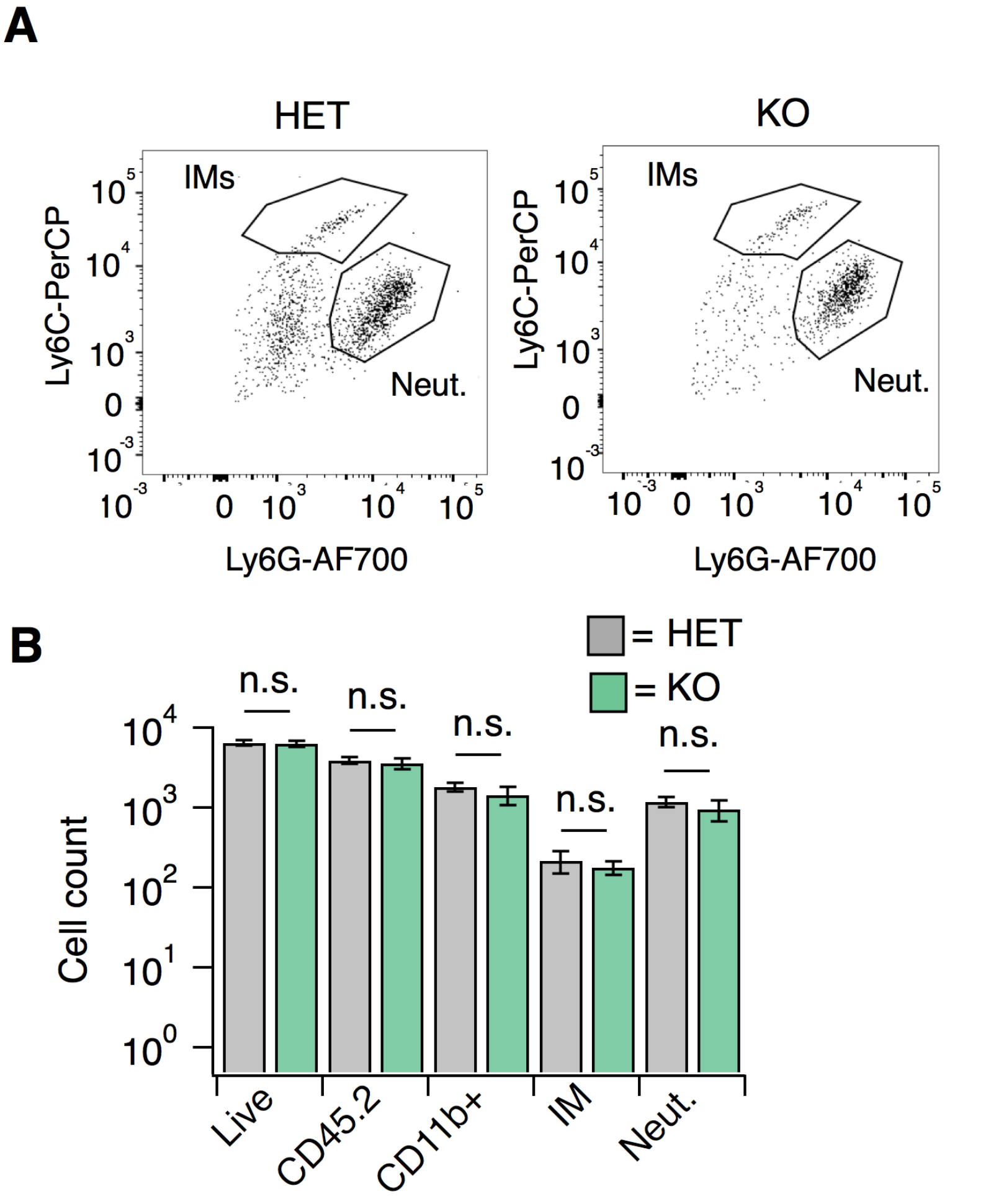

Figure 7-figure supplement 1

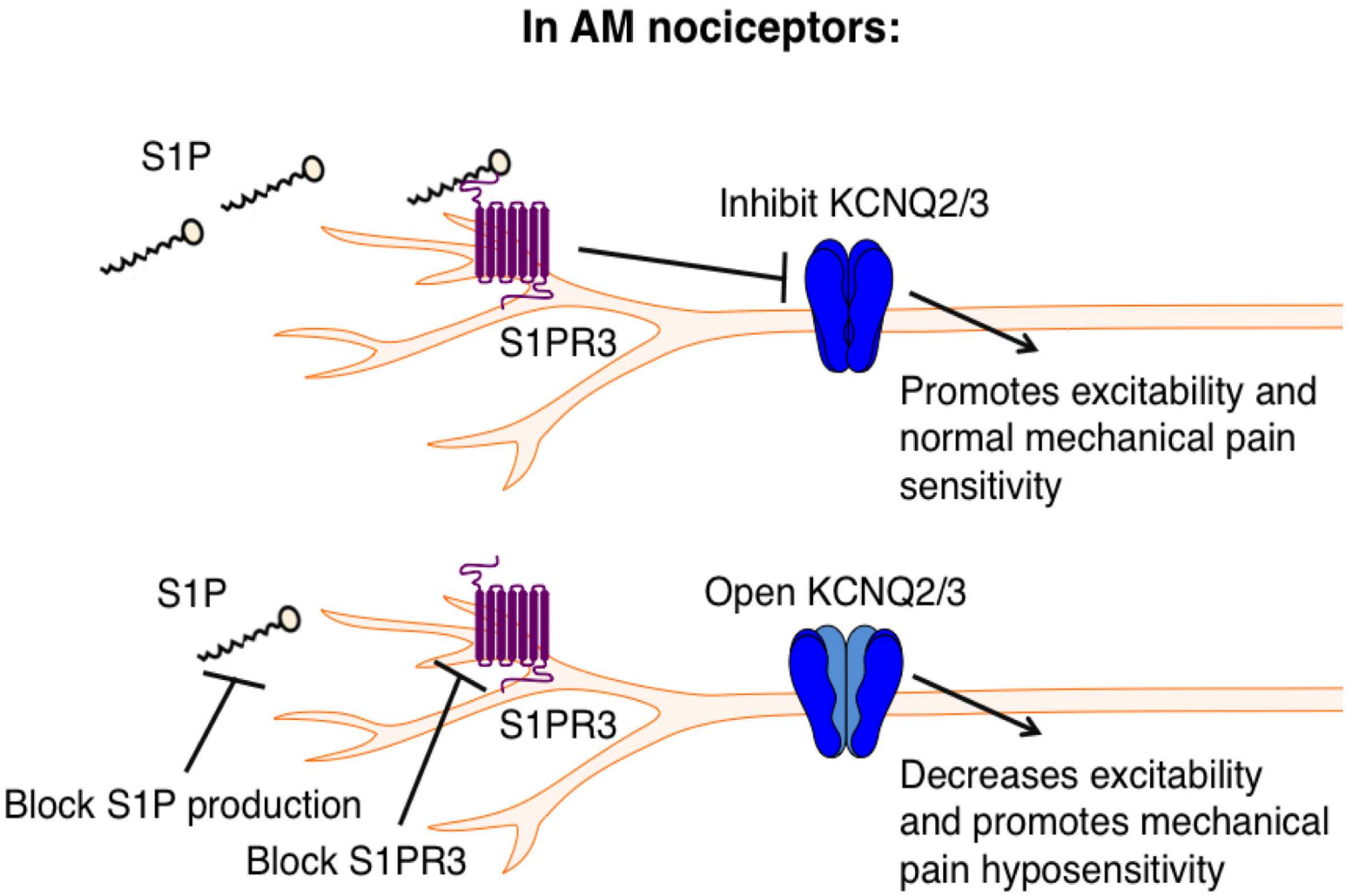
In AM nociceptors:
S1P
Inhibit KCNQ2/3
S1PR3
Promotes excitability and normal mechanical pain sensitivity
S1P
Open KCNQ2/3
S1PR3
Block S1P production
Block S1PR3
Decreases excitability and promotes mechanical pain hyposensitivity

Figure 8